TECHNICAL REPORT BRL-TR-3147

BRL

BLAST2D COMPUTATIONS OF THE REFLECTION OF PLANAR SHOCKS FROM WEDGE SURFACES WITH COMPARISON TO SHARC AND STEALTH RESULTS

DIXIE M. HISLEY

SEPTEMBER 1990

U.S. ARMY LABORATORY COMMAND

BALLISTIC RESEARCH LABORATORY
ABERDEEN PROVING GROUND, MARYLAND

NOTICES

Destroy this report when it is no longer needed. DO NOT return it to the originator.

Additional copies of this report may be obtained from the National Technical Information Service, U.S. Department of Commerce, 5285 Port Royal Road, Springfield, VA 22161.

The findings of this report are not to be construed as an official Department of the Army position, unless so designated by other authorized documents.

The use of trade names or manufacturers' names in this report does not constitute indorsement of any commercial product.

REPORT DOCUMENT PAGE

Form Approved
OMB No. 0704-0188

1. AGENCY USE ONLY *(Leave blank)*	2. REPORT DATE	3. REPORT TYPE AND DATES COVERED
	September 1990	Final, Jan 90 - Jul 90

4. TITLE AND SUBTITLE
BLAST2D Computations of the Reflection of Planar Shocks from Wedge Surfaces with Comparison to SHARC and STEALTH Results

5. FUNDING NUMBERS
1L162120AH25

6. AUTHOR(S)
Dixie M. Hisley

7. PERFORMING ORGANIZATION NAME(S) AND ADDRESS(ES)
U.S. Army Ballistic Research Laboratory
ATTN: SLCBR-TB-BD
Aberdeen Proving Ground, MD 21005-5066

8. PERFORMING ORGANIZATION REPORT NUMBER

9. SPONSORING/MONITORING AGENCY NAMES(S) AND ADDRESS(ES)
U.S. Army Ballistic Research Laboratory
ATTN: SLCBR-DD-T
Aberdeen Proving Ground, MD 21005-5066

10.SPONSORING/MONITORING AGENCY REPORT NUMBER
BRL-TR-3147

11. SUPPLEMENTARY NOTES
The sponsor for research for this report was U.S. Army Harry Diamond Laboratories, ATTN: SLCHD-NW-P, 2800 Powder Mill Road, Adelphi, MD 20783-1197.

12a. DISTRIBUTION/AVAILABILITY STATEMENT
Approved for public release; distribution is unlimited.

12b. DISTRIBUTION CODE

13. ABSTRACT *(Maximum 200 words)*

Computations of the reflection of planar shocks from wedge surfaces are performed with BLAST2D in order to compare to computational results from the SHARC, and the STEALTH codes and for comparison to experimental data obtained from the Ernst Mach Institut. Results are presented for an incident shock with Mach number equal to 2.12 impinging on 30, 45, and 60 degree wedges. Also, BLAST2D results are presented for an incident shock with Mach number equal to 1.295 impinging on a 25 and 60 degree double wedge for comparison to SHARC results and to an experimental shadowgraph published by Takayama and Ben-Dor. A new type of contour plot "the computational shadowgraph" is shown to produce excellent agreement with the experimental shadowgraph for the double wedge case.

14. SUBJECT TERMS
Mach reflection, inverse Mach reflection, BLAST2D, SHARC, STEALTH, computer simulation, planar shocks, wedges

15. NUMBER OF PAGES
92

16. PRICE CODE

17. SECURITY CLASSIFICATION OF REPORT	18. SECURITY CLASSIFICATION OF THIS PAGE	19. SECURITY CLASSIFICATION OF ABSTRACT	20. LIMITATION OF ABSTRACT
UNCLASSIFIED	UNCLASSIFIED	UNCLASSIFIED	UL

INTENTIONALLY LEFT BLANK.

ACKNOWLEDGEMENTS

This author wishes to thank Dr. Heilig, Mr. R. Lottero and Mr. J. Wortman for providing STEALTH and SHARC results for comparison to BLAST2D. In addition, the author wishes to thank Dr. Pieter Buning for modifying PLOT3D to provide the shadowgraph contouring capability.

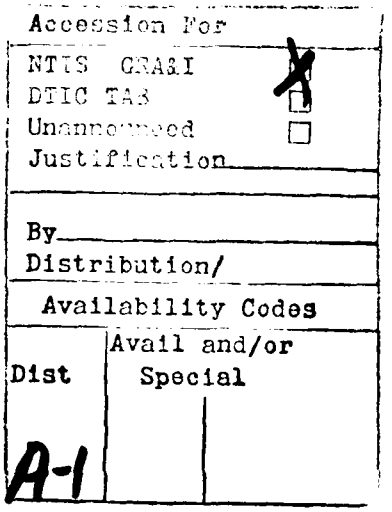

INTENTIONALLY LEFT BLANK.

TABLE OF CONTENTS

INTENTIONALLY LEFT BLANK.

LIST OF FIGURES

LIST OF FIGURES (Continued)

I. INTRODUCTION

1. Background

Mach reflection phenomenon is of interest to the Army because of its occurrence in simulations of blast wave interactions typical of nuclear explosions. A nuclear explosion releases a spherical blast wave that interacts with the ground producing Mach reflection patterns similar to the patterns produced when a planar shock impinges an inclined surface. For planar shock and wedge interactions, Mach reflection patterns are dominated by a combination of the following discontinuities: an incident shock, a reflected shock, a Mach stem, slip surfaces, and an expansion wave from the wedge leading edge. The region between the Mach stem and the slip surface is a region of high dynamic pressure. Typically one thinks of the crushing effect of the incident blast wave as the primary defeat mechanism of tactical equipment experiencing a nuclear explosion, but a secondary mechanism, the overturning effect caused by high dynamic pressure regions, must also be considered and Army equipment hardened for survivability.

An extensive amount of experimental, theoretical and computational data has been published (1-4) for the reflection of planar shocks from various inclined rigid surfaces. The wealth of qualitative and quantitative data available, and the similarity to blast wave phenomenology, makes the simulation of the reflection of planar shocks from wedge surfaces a good choice for computer code verification and comparison. Three gas dynamic codes, BLAST2D, SHARC, and STEALTH were run for several planar shock/wedge geometries and initial conditions and their results compared.

The reflection of planar shocks from a sharp compressive corner can take on one of four psuedo-stationary (self-similar) patterns, regular reflection (RR), single Mach reflection (SMR), complex Mach reflection (CMR), or double Mach reflection (DMR). The pattern that results depends on the wedge angle, the incident shock Mach number, and the gas equation of state. Figure 1 presents the transition boundaries between the different reflection patterns for air with a perfect gas equation of state. For the cases presented here, Mach number approximately equal to 2, regular reflection, single Mach reflection, and complex Mach reflection are the dominant patterns. Schematics of these patterns are also shown in Figure 1.

Additionally, a shock impinging on a double wedge was computationally simulated with BLAST2D for comparison to an experimental shadowgraph and SHARC results. When the planar shock impinges the first wedge, a direct single Mach reflection occurs. However, when the single Mach reflection system impinges the second wedge an inverse Mach reflection results. The interesting feature of an inverse Mach reflection is that its triple point propagates toward the wedge surface, and eventually reflects from the wedge surface producing a complex wave pattern mainly dominated by a regular reflection pattern.

Takayama and Ben-Dor (5) and Ben-Dor et al.(6) published experimental shadowgraphs which show the details of the inverse Mach reflection process. Dawson et al.(7) published a SHARC computational simulation of the the double wedge case in which the major features of

the complex wave pattern were reproduced in a density contour plot, but some of the slip lines revealed in an experimental shadowgraph were not computationally captured. Capturing gradients through contour plots requires adequate grid resolution for the problem and an adequate choice of grid contour levels. In addition, experimental shadowgraphs are based on the second derivatives of density, therefore, computational shadowgraphs, similarly based on the second derivatives of density, were generated using spatially and temporally second-order accurate BLAST2D results to see if all the slip lines could be revealed. This is the first time to this author's knowledge that computational shadowgraphs for wedge problems have been published.

2. Objectives

The objectives of this report are to compare results from BLAST2D to results obtained with the STEALTH and SHARC codes for shocks with Mach number equal to 2.12 impinging on single wedges. Grid resolution effects will be examined. Contour plots and pressure versus time histories will be compared. Also, a BLAST2D computation was performed for the double wedge case to see if the complex inverse Mach reflection pattern produced experimentally and reproduced partially by a SHARC density contour plot could be fully captured by BLAST2D results and a computational shadowgraph contour plot. A discussion of the BLAST2D code follows but for more information on the STEALTH and SHARC codes the reader should consult references 8 and 9.

II. THE BLAST2D CODE

1. Governing Equations

The governing equations for the blast problems presented here are the two-dimensional unsteady Euler equations, written in integral form:

$$\frac{d}{dt}\int_{\mathcal{V}} Q d\mathcal{V} + \int_{S} n \cdot F dS = 0 \tag{1}$$

The integral form of the Euler equations can be rewritten for a two-dimensional generalized cell volume as:

$$0 = \frac{d}{dt}\int_{\mathcal{V}} Q d\mathcal{V} + \int_{j-1/2}^{j+1/2} \left(E_{i+1/2} - E_{i-1/2}\right) d\eta + \int_{i-1/2}^{i+1/2} \left(F_{j+1/2} - F_{j-1/2}\right) d\xi \tag{2}$$

where

$$Q = \begin{pmatrix} \rho \\ \rho u \\ \rho v \\ e \end{pmatrix}, \quad E = \begin{pmatrix} \rho U \\ \rho U u + y_\eta p \\ \rho U v - x_\eta p \\ (e+p)U \end{pmatrix}, \quad F = \begin{pmatrix} \rho V \\ \rho V u - y_\xi p \\ \rho V v + x_\xi p \\ (e+p)V \end{pmatrix} \tag{3}$$

This set of four integral equations represents the conservation of mass, momentum in x and y directions, and energy, per unit volume where ρ is the density, p is the pressure, u and v are the velocities in the x (longitudinal) and y (height) directions respectively, and e is the total internal energy per unit volume:

$$e = \frac{p}{(\gamma - 1)} + 1/2\ \rho(u^2 + v^2) \tag{4}$$

The volume fluxes are defined as:

$$U = y_\eta u - x_\eta v \tag{5}$$

$$V = y_\xi u + x_\xi v \tag{6}$$

For a two-dimensional cell, the integration of flux over the surface in Equation 1 has been replaced in Equation 2 by an integral over each face of the cell. The η-direction is taken as the body normal and the ξ-direction is tangential to the surface of the body. The cell volume and walls are assumed to be fixed in time. The metrics $x_\xi, y_\xi, x_\eta, y_\eta$ are the vector elements of the cell walls and $\mathcal{V}$ is the volume of the grid cell.

The physical, independent variables (x,y,t) were transformed into a uniformly spaced computational grid (ξ, η, τ) by a general transformation of the form:

$$\begin{aligned} \tau &= t \\ \xi &= \xi(t, x, y) \\ \eta &= \eta(t, x, y) \end{aligned} \tag{7}$$

The transformations were chosen so that the grid spacing in the computational space is uniform and of unit length, $\Delta\xi = 1$, $\Delta\eta = 1$. Thus, the uniform equi-spaced mesh in ξ and η allows the use of unweighted differencing schemes. As a result, the computational code can be applied to a variety of physical geometries and grids.

If an average flux is defined on the cell faces, and $\Delta\xi$ and $\Delta\eta$ are taken as unity, the integral form of the Euler equation, Equation 2 can be rewritten in finite volume form as:

$$\mathcal{V}_{i,j} \frac{Q^{n+1}_{i,j} - Q^n_{i,j}}{\Delta\tau} + \frac{\hat{E}^m_{i+1/2,j} - \hat{E}^m_{i-1/2,j}}{\Delta\xi} + \frac{\hat{F}^m_{i,j+1/2} - \hat{F}^m_{i,j-1/2}}{\Delta\eta} = 0 \tag{8}$$

where the indices i and j correspond to the ξ and η directions respectively in the computational mesh.

The vectors $\hat{E}$ and $\hat{F}$ are the convective numerical fluxes in computational space (ξ, η, τ) consistent with the physical fluxes E and F in (x,y,t). The vector $\bar{Q}$ consists of the cell

averaged dependent variables. The integration scheme is fully implicit if m=n+1 and is explicit if m=n. The variables have been nondimensionalized as follows;

$$\tilde{x} = \frac{x}{L} \qquad \tilde{u} = \frac{u}{c_1} \qquad \tilde{p} = \frac{p}{\rho_1 c_1^2}$$

$$\tilde{y} = \frac{y}{L} \qquad \tilde{v} = \frac{v}{c_1} \qquad \tilde{e} = \frac{e}{\rho_1 c_1^2} \tag{9}$$

$$\tilde{\rho} = \frac{\rho}{\rho_1} \qquad \tilde{t} = \frac{t c_1}{L}$$

where L=1, c=sound speed, and subscript 1 represents the ambient conditions initially present in the driven section.

2. The Computational Algorithm

The fine grid computations were performed on a Cray XMP/48 supercomputer and the coarse grid computations on an IRIS4D workstation by discretizing the Euler equations with an upwind, Total Variation Diminishing (TVD), finite-volume, implicit scheme. In previous papers, the scheme was presented in detail and proved to be well suited for blast wave calculations (10,11). For a complete mathematical description of the algorithm, the reader is referred to these reports. The remainder of this section contains a description of the characteristics of the algorithm in general terms.

The BLAST2D algorithm is based upon Roe's approximate Riemann solver (12) coupled with upwind flux difference splitting. Other approximate Riemann solvers could have been used, but Roe's method is the approach recommended by Chakravarthy when computational efficiency is important (13). The Riemann problem is given two initial states and the dependent variables at the center of two neighboring control volumes for a finite volume formulation, compute the wave families (that is the combination of shocks, contacts, and rarefaction fans) that result at the interface of the control volumes. Roe's technique provides a direct approximation of the intermediate states in contrast to a solution of the exact Riemann problem which requires an iterative process.

Once the piecewise constant states separated by the wave families are determined, the flux differences across each wave family can be computed. Upwinding requires that the flux differences across right running wave families (positive eigenvalues) be used in the derivative evaluations of fluxes into neighboring fluid cells to the right of the Riemann solution and that the flux differences across left running wave families (negative eigenvalues) be used in the derivative evaluations of fluxes into neighboring fluid cells to the left. In this way a method of characteristics-like flavor is brought into the numerical algorithm. Flux difference splitting with TVD was used to achieve second-order accuracy without introducing spurious oscillations near discontinuities.

The second-order convective flux was produced by adding a correction term to the first-order flux. However, in order to avoid spurious oscillations, the correction term must

fulfill the criteria for the algorithm to be TVD. TVD schemes achieve second-order accuracy without introducing spurious oscillations near discontinuities by employing a feedback mechanism- 'smart numerical dissipation'- wherein fluxes are compared at neighboring control volumes. In regions of little change no numerical dissipation is added to the second order correction terms, while in regions of large change, numerical dissipation is added to ensure numerical stability.

During this process new extrema are not created by the numerical dissipation. TVD data preserve monotonicity; a) no new numerical extrema is created and b) the absolute value of already existing numerical extrema must not increase. TVD schemes have been rigorously proven in one dimension, however the extensions to two and three dimensions have not been mathematically proven. The advantages of TVD algorithms over older schemes are that strong gradients and complex flow fields are resolved accurately without the need to adjust arbitrary smoothing parameters. The disadvantages of upwind differencing with TVD are long computing times caused by an increase in the number of arithmetic operations per integration step and loss of programming simplicity.

The conservative nature of the scheme captures shocks and other discontinuities automatically. The finite volume philosophy ensures conservation at interior and boundary points. The scheme is made implicit by linearizing only the first-order contribution and by employing a Newton iteration of the type described by Rai (14) to eliminate any approximations made. The implicit version of the scheme requires more computations per integration step than the explicit version, but is necessary to handle the stiff nature of the problems.

The discussion in this section assumed the reader was familiar with state-of-the-art computational fluid dynamic terms and definitions. Others are urged to read the reports referenced in this section for a full mathematical description.

III. GEOMETRY, GRID, AND INITIAL CONDITIONS FOR WEDGE COMPUTATIONS

Computations with BLAST2D were performed for the wedge configurations and initial conditions shown in Figures 2 and 3. All dimensions given are in centimeters. Figure 2 shows the geometries for the single wedge cases while Figure 3 shows the geometry for the double wedge case. Figure 2(A) was run with a 189×172 grid for comparison to the SHARC code. Figures 2(B), 2(C), and 2(D) were run with 98×25, 46×25, and 68×25 grids respectively for comparison to the STEALTH code. The shock was initialized one centimeter in front of the start of the wedge for case (A) and two centimeters in front of the leading edge of the wedge for cases (B), (C), and (D). Figure 3 was run with a 200×200 grid for comparison to the SHARC code and the shock was initialized at x=.40 centimeters. The geometries and grids were chosen to reproduce simulations already completed by Heilig (15), Lottero and Wortman (16), and Dawson et al. (7) using the STEALTH and SHARC codes.

IV. RESULTS AND DISCUSSION

1. 30 Degree Wedge - 98×25 grid

Figure 4 presents BLAST2D density and pressure contours superimposed on the computational grid (black lines) for a shock with Mach number equal to 2.12 impinging on a 30 degree wedge. The contour data is normalized by conditions in front of the shock and is shown at 171 microseconds from the start of the calculation. The calculation was started at time zero with the shock one centimeter in front of the leading edge of the wedge. For this geometry and initial shock, a single Mach reflection results. Even at this coarse resolution the slip line is resolved in the density contours, but is too diffuse for accurate angle measurements and comparison to von Neumann theory. The slip line is defined as a streamline where the flow on either side has the same static pressure and flow direction, however, the density, velocity magnitude, temperature, and other related functions are different.

The slip line is more clearly seen in Figures 5 and 6 which present contour plots of Mach number, velocity magnitude, temperature, speed of sound, dynamic pressure, entropy, shadowgraph function, and vorticity magnitude. Appendix A presents equations for these functions. Perhaps the most interesting of these plots is the dynamic pressure plot. Clearly the region between the Mach stem and the slip line is the region of highest dynamic pressure. The Army is especially interested in this region because the high dynamic pressure can overturn and translate vehicles and equipment, diminishing their survivability in the event of a nuclear explosion.

The shadowgraph function is the second derivative of density in each direction added together. However, beause the grid is coarse, the discontinuities in the computational shadowgraph are extremely smeared. As shown by the 189×172 grid shadowgraph contour plot, higher grid resolution produces computational shadowgraphs that are comparable to the resolution seen in experimental shadowgraphs.

In simple terms, entropy is a measure of the disorder of the system, the higher the entropy, the greater the disorder. The highest entropy region, shown in Figure 6, is the region between the Mach stem and the slip line. The vorticity magnitude plot, Figure 6, shows this region to have the highest vorticity which indicates rotational flow present. Flow regions with zero vorticity magnitude are irrotational. A major difference between the low resolution contour plots just examined and the high resolution plots discussed in the next section is the low resolution plots indicate the entire region between the Mach stem and the slip line to be rotational, while the high resolution plots show only the slip line and a small area behind the Mach stem as rotational. The higher resolution case discussed next, in the absence of viscous effects, should provide more accurate results.

2. 30 Degree Wedge - 189×172 grid

Figure 7 presents BLAST2D density and pressure contours superimposed on grid lines for a fine resolution run. Only every other grid line is plotted for clarity. The most significant feature of the finer resolution is all discontinuities are captured more accurately. The angles between the discontinuities were measured and are in excellent agreement with Von Neumann values as reported by Heilig (15). Figure 8 presents Mach number, velocity magnitude, temperature and speed of sound contours. Qualitatively, the plots appear to produce correct trends. Figure 9 presents dynamic pressure, entropy, shadowgraph function, and vorticity magnitude contours. The dynamic pressure contour shows the roll-up of the slip line as the highest dynamic pressure region. This is the region, discussed earlier, that is responsible for overturning.

3. 30 Degree Wedge - Contour Plot Comparisons

Figure 10 presents a comparison of BLAST2D and SHARC contour plots for the 189×172 grid. In order to grid the wedge, SHARC is restricted to island, that is rectangular solid cells, or shore cells which are rectangular cells split along either diagonal and half of which is treated as solid and the other half as fluid. By choosing the proper aspect ratio rectangles and using shore cells, SHARC could model a smooth wedge surface of the required slope for the thirty degree wedge. The grid for BLAST2D is a body conformal grid produced using an elliptic grid generation code.

Both codes appear to resolve the discontinuities present, however, the slip line captured by SHARC is not as crisply defined. Also, the slip line produced by SHARC appears to turn into the Mach stem with an unrealistic clustering of the contour lines. Lottero and Wortman are investigating the cause of this inaccuracy, which may be a plotting error in the postprocessing routines. Both codes show some contour lines that are numerical noise in front of the incident shock. However, the noise does not show up in pressure-versus time histories and is not considered significant.

Figure 11 presents a comparison of contours generated by BLAST2D and the STEALTH code with similar resolution in the y direction, however the x direction resolution is ambiguous in the case of STEALTH because the grid points move for this Lagrangian calculation. It is clear that the contours produced by STEALTH are not as crisply defined as either BLAST2D or SHARC. However, it should be noted that STEALTH was rezoning in this computation. This could be a source of inaccuracy. There is no reason to believe that STEALTH numerics alone are responsible for the poorly defined results. One would not normally choose a Lagrangian code for this type of computation.

4. 30 Degree Wedge - Pressure versus Time Comparisons and Surface Density Plots

Figures 12-14 show the effects of grid resolution on pressure versus time histories as well as a comparison of BLAST2D, STEALTH and SHARC results. Positions A-F are experimental probe locations as reported by Heilig (15): Position A, x=12.250, y=-9.0672, Position B, x=12.250, y=-4.3365, Position C, x=12.250, y=-0.78845, Position D, x=18.500, y=-5.7474, Position E, x=18.500, y=-2.7488, Position F, x=18.500, y=-0.49977. The y values are subtracted from 10, the overall height of the computational domain, to get the positive y positons. The leading edge of the wedge was defined by Helig as x=12.0, y=0.0. For the SHARC comparisons, Lottero and Wortman (16) defined the relative positions to the leading edge to be the same, but the leading edge was defined as x=0.0, y=0.0. As expected, the finer grid resolution produces sharper discontinuities, that is, discontinuities with less rise time. The various codes seem to be in reasonable agreement for the same resolution with one exception. The STEALTH code produces a rise in pressure at Position B that occurs at a much earlier time, 100 microseconds, than BLAST2D or SHARC, 190 microseconds. Position B was either incorrectly reported, or incorrectly placed for the STEALTH run. BLAST2D has the least oscillatory nature at discontinuities, nevertheless all codes are in very good agreement with experimental results shown as solid lines.

Surface density results from BLAST2D are presented in Figure 15 for the coarse and fine resolutions run. The fine resolution captures discontinuities with smaller rise times, however the coarse resolution also does an excellent job of reproducing the correct overall pressure levels and trends. Both resolutions are in excellent agreement with Von Neumann theory for ρ_4/ρ_1 and ρ_3/ρ_1.

5. 45 Degree Wedge - 68×25 grid, 60 Degree Wedge - 46×25 grid

The 45 and 60 degree wedge cases were run using BLAST2D for comparison to STEALTH results. The grids were chosen to closely approximate the starting grids used with STEALTH. Figures 16 and 17 present density and pressure contour comparisons for these wedge angles. The 45 degree case was expected to produce a complex Mach reflection, however, only a single Mach reflection pattern was discernible from the contour plots. A kink clearly can not be seen in Figure 16. Using a fine grid resolution, and a second order Godunov scheme Glas et al. (1), also produced contour plots for this case which did not show a clearly discernible kink, however, when they increased the Mach number of the shock from 2.1 to 2.3 and used the same fine resolution, a kink appeared. In general, Figures 16 and 17 show that the contour plots produced by STEALTH are more noisy than those produced by BLAST2D, but more disturbing is the STEALTH density contour plot for the 60 degree wedge case showed an attached shock at the corner of the wedge which is unrealistic. BLAST2D at the same resolution, and SHARC on a higher resolution grid (16), showed no evidence of an attached shock.

Figures 18 and 19 present BLAST2D and STEALTH snapshots of the pressure along a

constant j grid line for the 45 and 60 degree wedge cases respectively. Also, Von Neumann predictions are plotted for reference. Both codes appear to do a good job of predicting the overall pressure level behind the incident and reflected shocks. Surface density plots were computed for BLAST2D results and are presented in Figures 20 and 21 for completeness.

6. 25 and 60 Degree Double-Wedge - 199×199 grid

Figure 22 presents the density contour plot computed using BLAST2D results at 308 microseconds for the double wedge case. Initially, the incident shock reflects over the first wedge surface as a single Mach reflection. The Mach stem created by the first wedge reflects from the second wedge as another single Mach reflection. Later the triple point from the first wedge reflection process and the triple point from the second wedge combine to form one single Mach reflection pattern which moves toward the wedge surface and is termed an inverse Mach reflection. The inverse Mach reflection occurs because the second effective wedge angle is such that it cannot support stationary or direct Mach reflection. For stationary Mach reflection the triple point moves parallel to the wedge surface and for direct Mach reflection the triple point moves away from the wedge surface.

When the inverse Mach reflection collides with the wedge surface, a regular reflection pattern results. Figure 22 shows the density contour plot produced by BLAST2D for the complex pattern that results after the collision of the inverse Mach reflection with the wedge surface. When this figure is compared to the experimental shadowgraph in Figure 23, one notices three slip lines in the experimental shadowgraph that are not clearly indicated in the density contour plot.

Dawson et al. published (7) a density contour plot for the same case using SHARC which also did not capture the slip lines. Probably, adequate grid resolution and contour levels were used, but gradient plots were not published. When a density gradient magnitude contour plot was computed using BLAST2D, Figure 24, two of the slip lines are resolved, and furthermore when a shadowgraph function contour plot, Figure 25, was produced, all gradients of interest were resolved. It is interesting to note that in the experimental shadowgraph, one does not get a good appreciation of the differing strengths associated with each of the discontinuities. However, the computational shadowgraph shows that the third slip line is bounded by contour levels that are very close to ambient levels.

V. CONCLUSIONS

To conclude, for sharp accurate rise-times, a fine grid is required, while for pressure level trends, a coarse grid is adequate. Also, finer resolution showed the roll-up of the slip line for the 30 degree wedge case to be a region of high dynamic pressure, instead of the entire region between the Mach stem and the slip line as indicated by the coarser resolution.

Shadowgraph function contour plots should be used to resolve slip lines that are too small to be seen in density and density gradient contours. The shadowgraph function contour

plot should provide the best comparison to experimental shadowgraphs provided the grid resolution is fine enough that discontinuities do not become smeared.

BLAST2D captures slip lines very well and is the least oscillatory of the three codes compared. BLAST2D has the advantages that grids can be body conformal, and that it is constructed with total variation diminishing (TVD) concepts to not produce numerical overshoots, but has the disadvantage that it is computationally more expensive to run for the same grid resolution. However, as shown by the 30 degree wedge runs BLAST2D produces very good results even on coarse grids. STEALTH produced an unrealistic attached shock for the 60 degree wedge case at coarse resolution which neither BLAST2D using a coarse resolution or SHARC using a finer grid produced. SHARC has the disadvantages of numerical overshoots unless artificial viscosity is turned on and judiciously chosen for the problem, that geometries must be approximated by shore and island cells but, is computationally less expensive to run than BLAST2D for the same resolution. As shown by the 30 degree wedge comparisons, the numerical overshoots with SHARC are significant while overshoots with BLAST2D are not discernible. One can see from a comparison of BLAST2D and SHARC that the trade-off one tries to optimize when running one computer code or another for a particular problem is degree of accuracy versus expense.

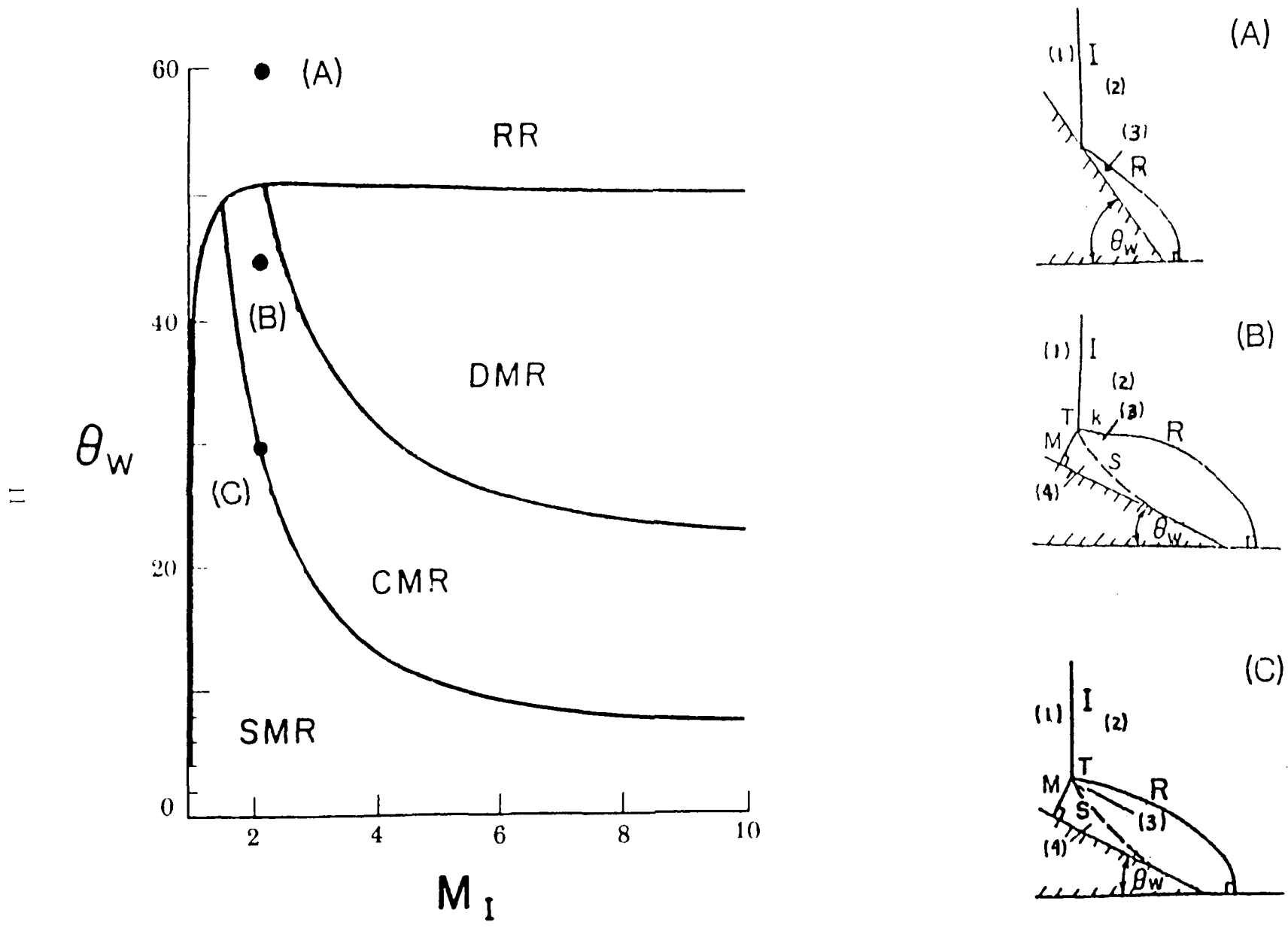

Figure 1. Single Mach Reflection (SMR), Regular Reflection (RR), and Complex Mach Reflection (CMR) Patterns and Transition Boundaries

INITIAL CONDITIONS: M_I = 2.12
p2= 45.7 kPa
p1= 9.0 kPa
R= 287 J/kg/K
gamma= 1.4

rho2= .3023 kg/m*3
rho1= .1064 kg/m*3
T2= 526.75 K
T1= 294.65 K
U2= 472.74 m/s

GEOMETRIES:

dimensions in cm

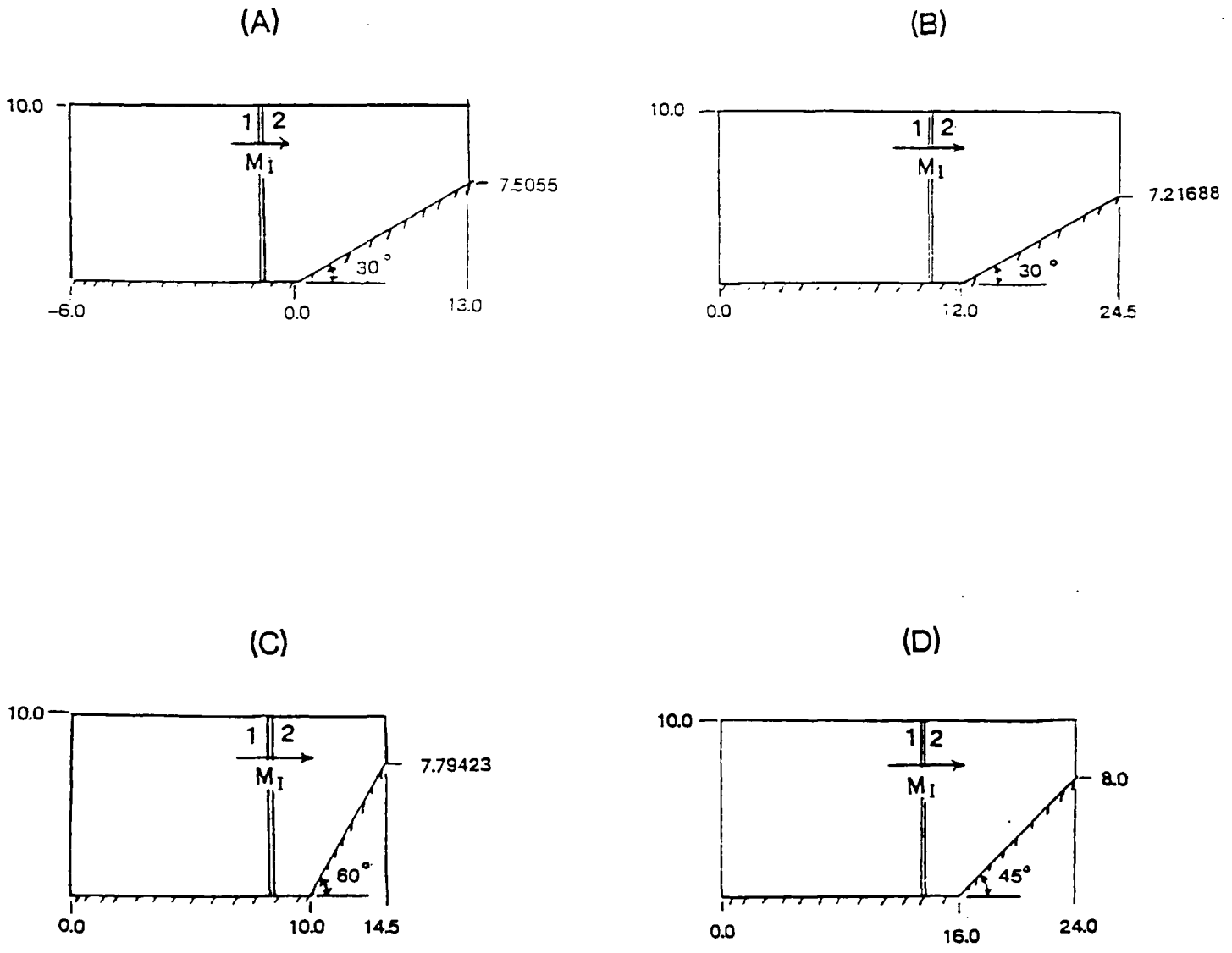

Figure 2. Wedge Geometries and Initial Conditions for Single Wedge Cases

INITIAL CONDITIONS: M_I= 1.295 rho2= 1.80 kg/m*3
p2= 181.94 kPa rho1= 1.183 kg/m*3
p1= 100.08 kPa T2= 352 K
R= 287 J/kg/K T1= 295 K
gamma= 1.4

DOUBLE-WEDGE GEOMETRY:
dimensions in cm

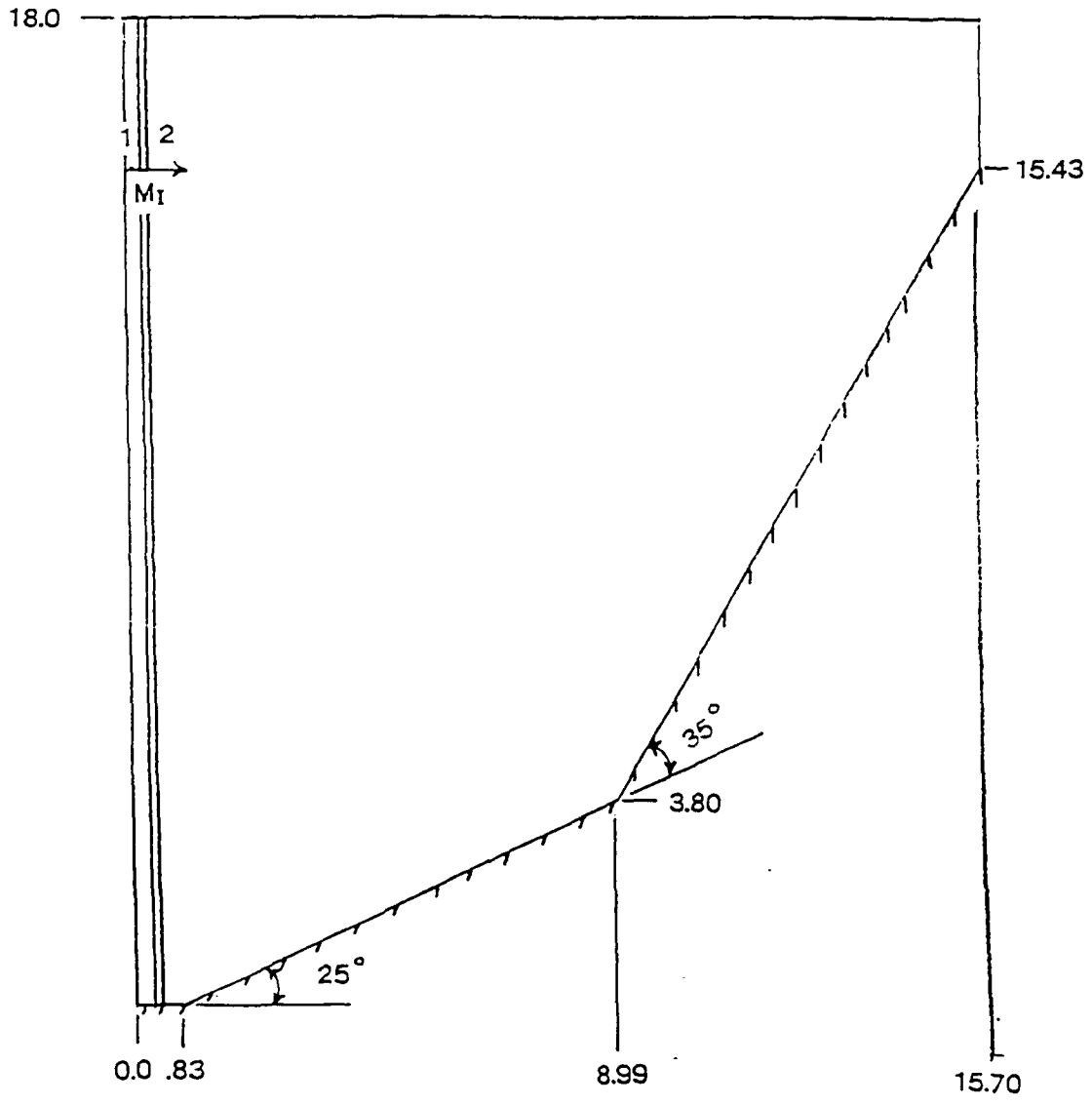

Figure 3. Wedge Geometry and Initial Conditions for Double Wedge Case

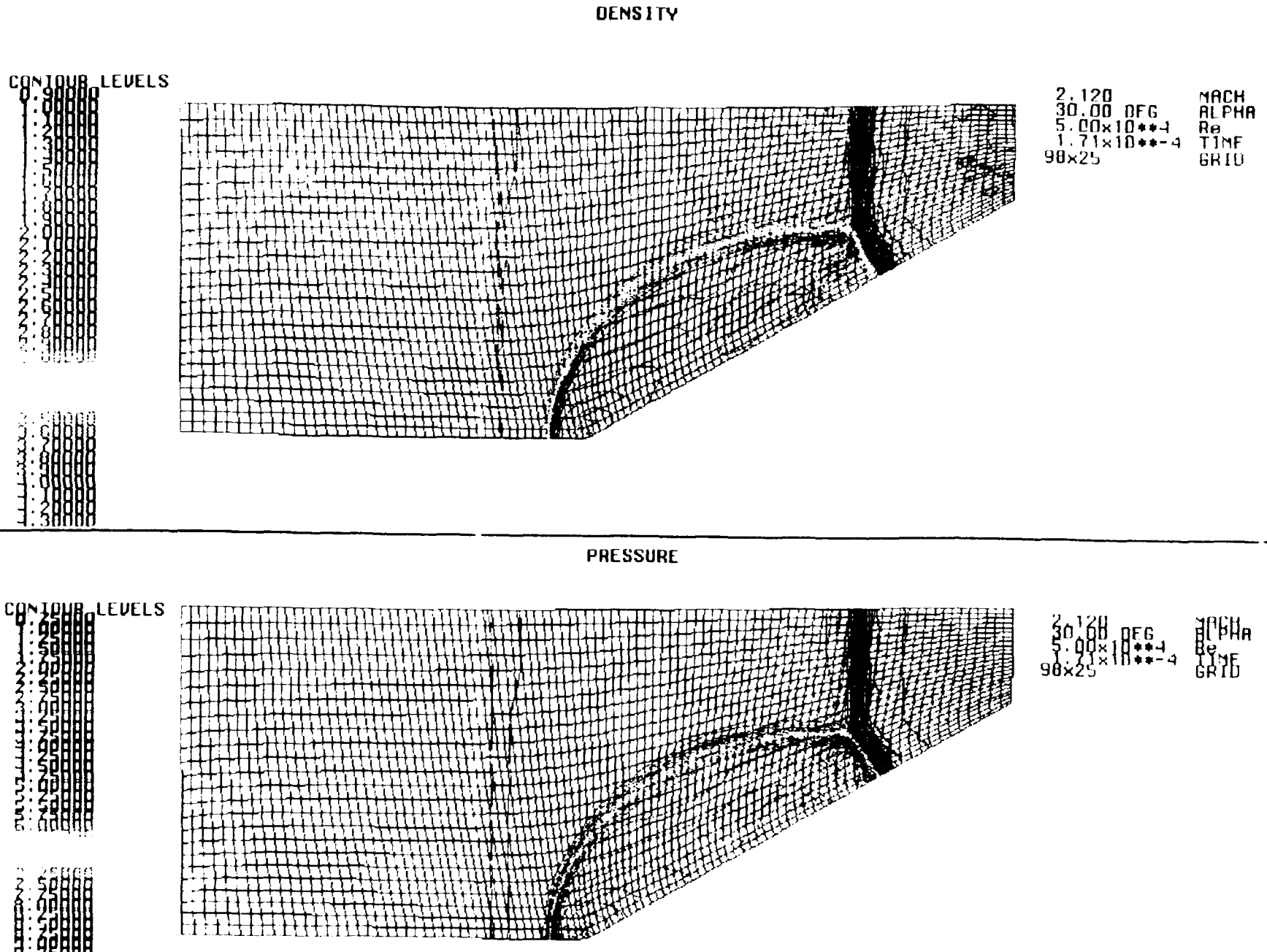

Figure 4. Density and Pressure Contours Superimposed on 98×25 Grid, $M_I = 2.12$, 30 Degree Wedge

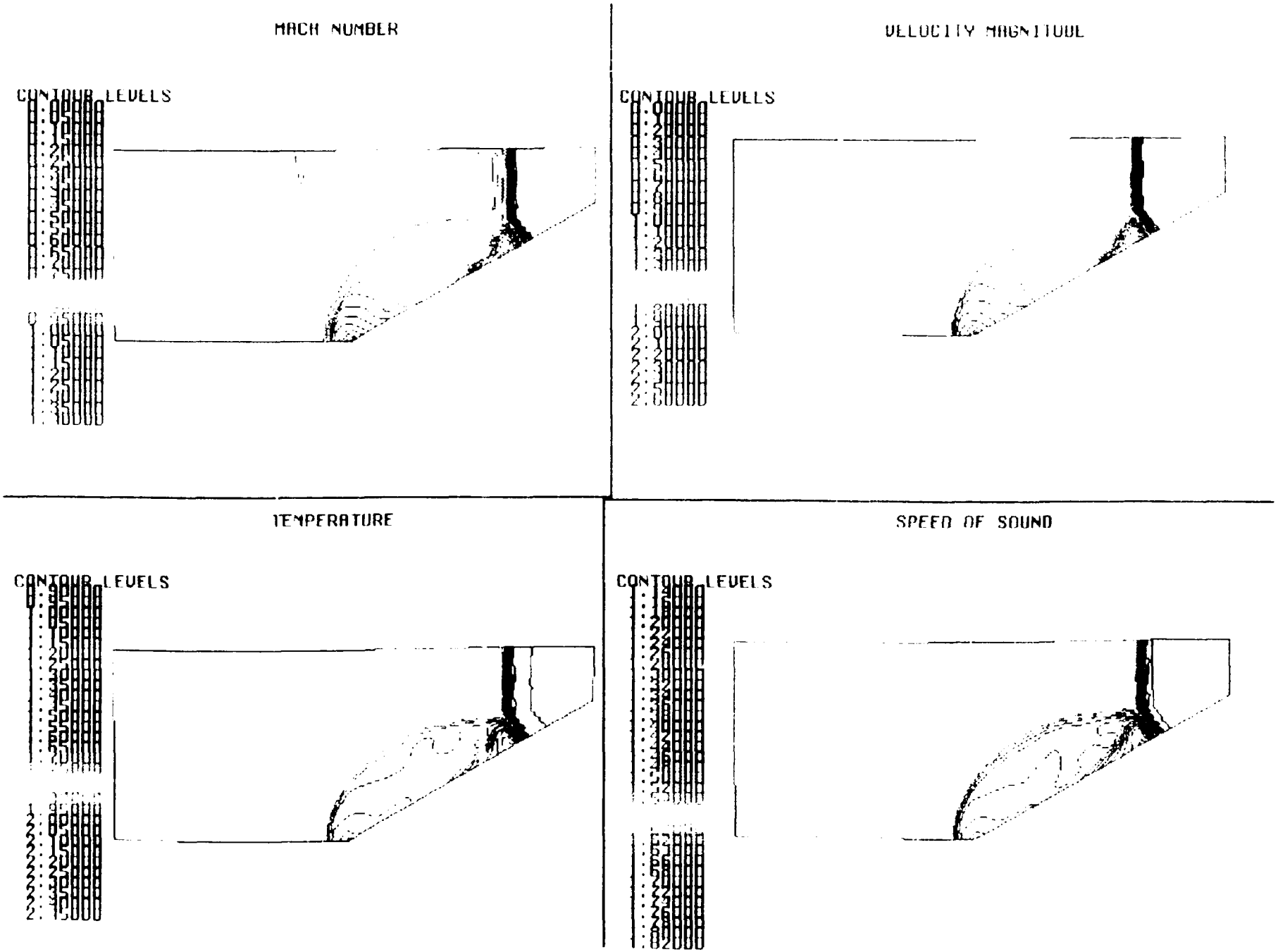

Figure 5. Mach Number, Velocity Magnitude, Temperature, and Speed of Sound Contours, $M_I = 2.12$, 30 Degree Wedge

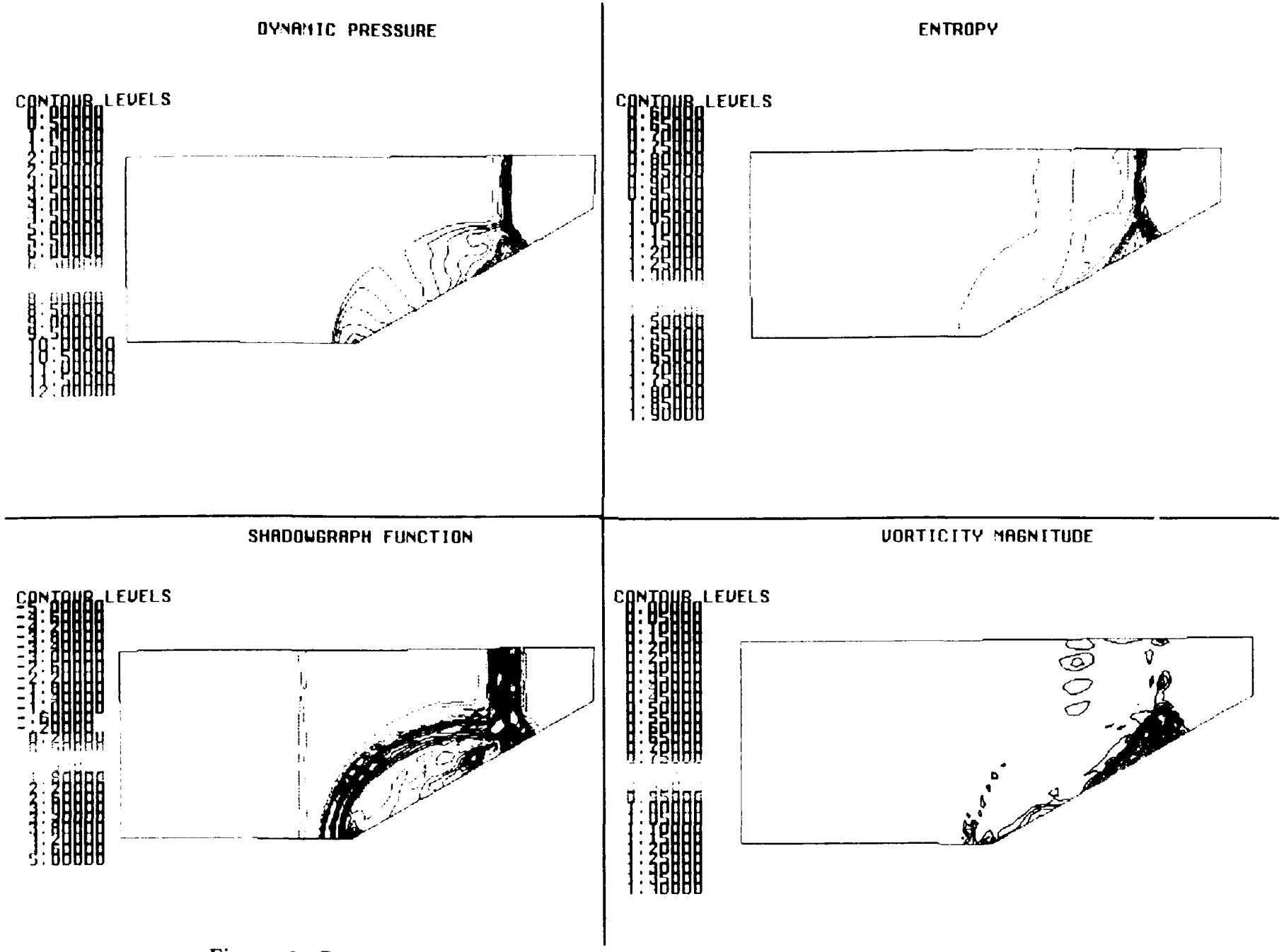

Figure 6. Dynamic Pressure, Entropy, Shadowgraph Function, and Vorticity Magnitude Contours, $M_I = 2.12$, 98×25 grid, 30 Degree Wedge

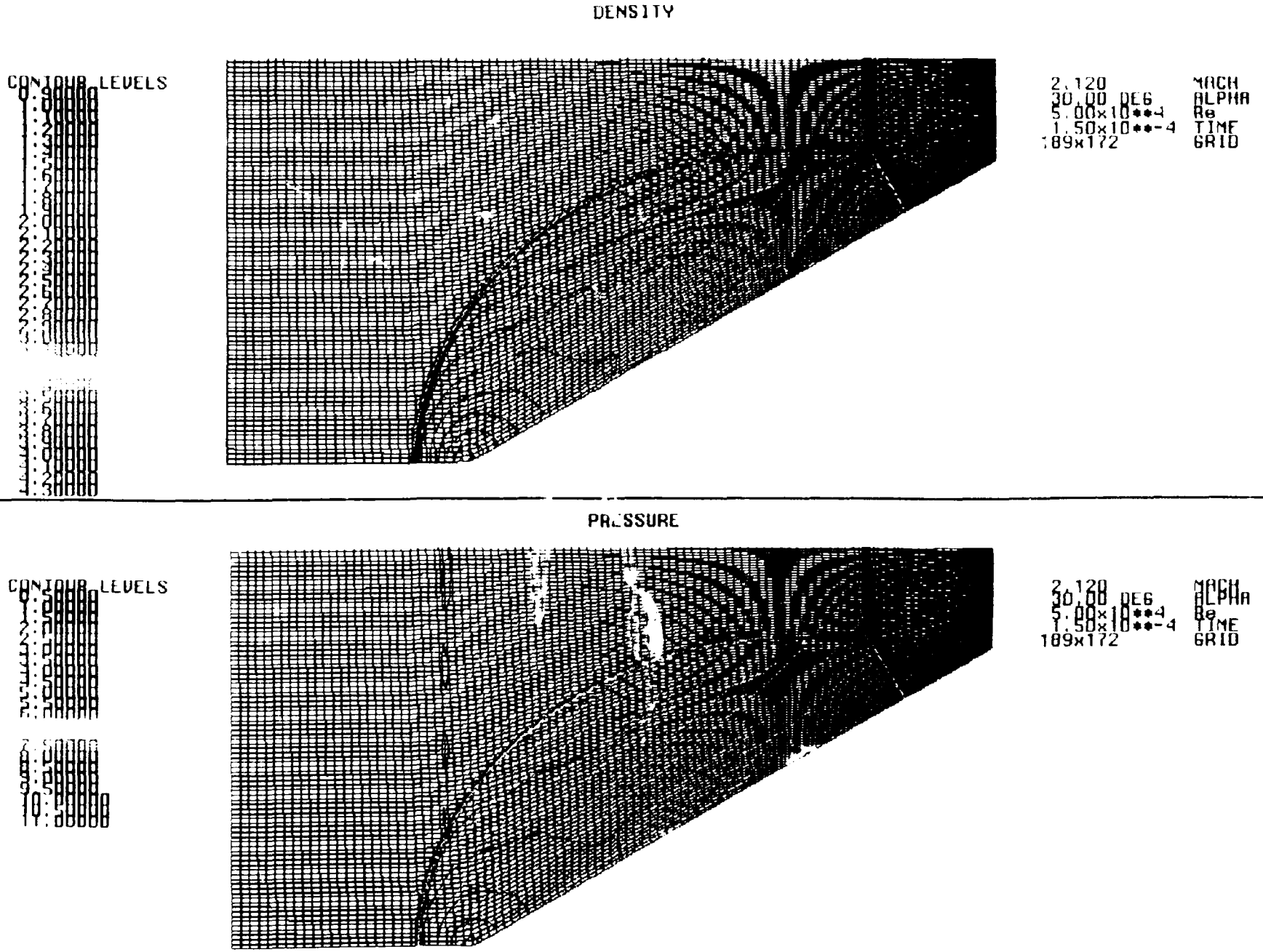

Figure 7. Density and Pressure Contours Superimposed on 189×172 Grid, $M_I = 2.12$, 30 Degree Wedge

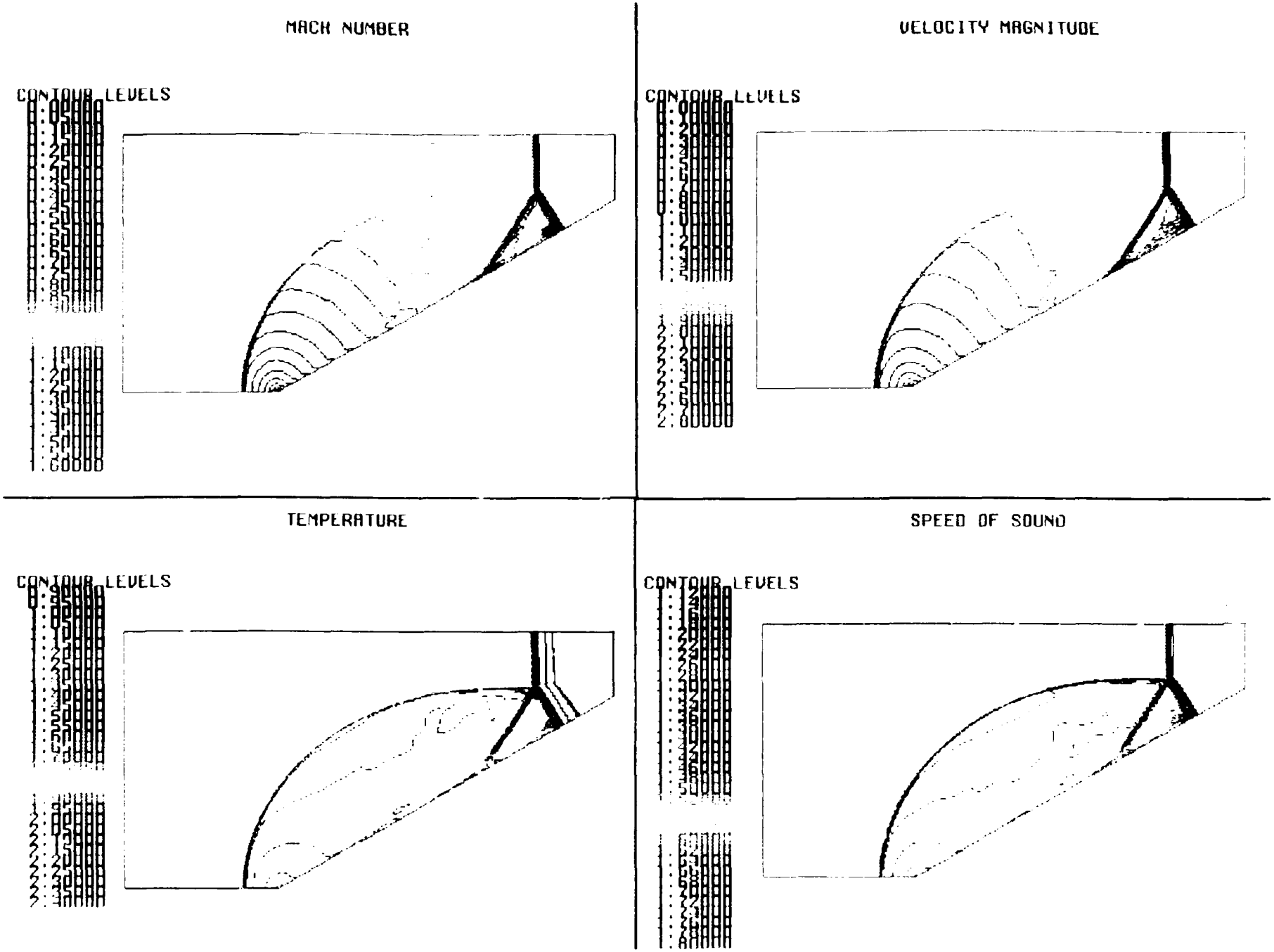

Figure 8. Mach Number, Velocity Magnitude, Temperature, and Speed of Sound Contours. $M_I = 2.12$, 30 Degree Wedge

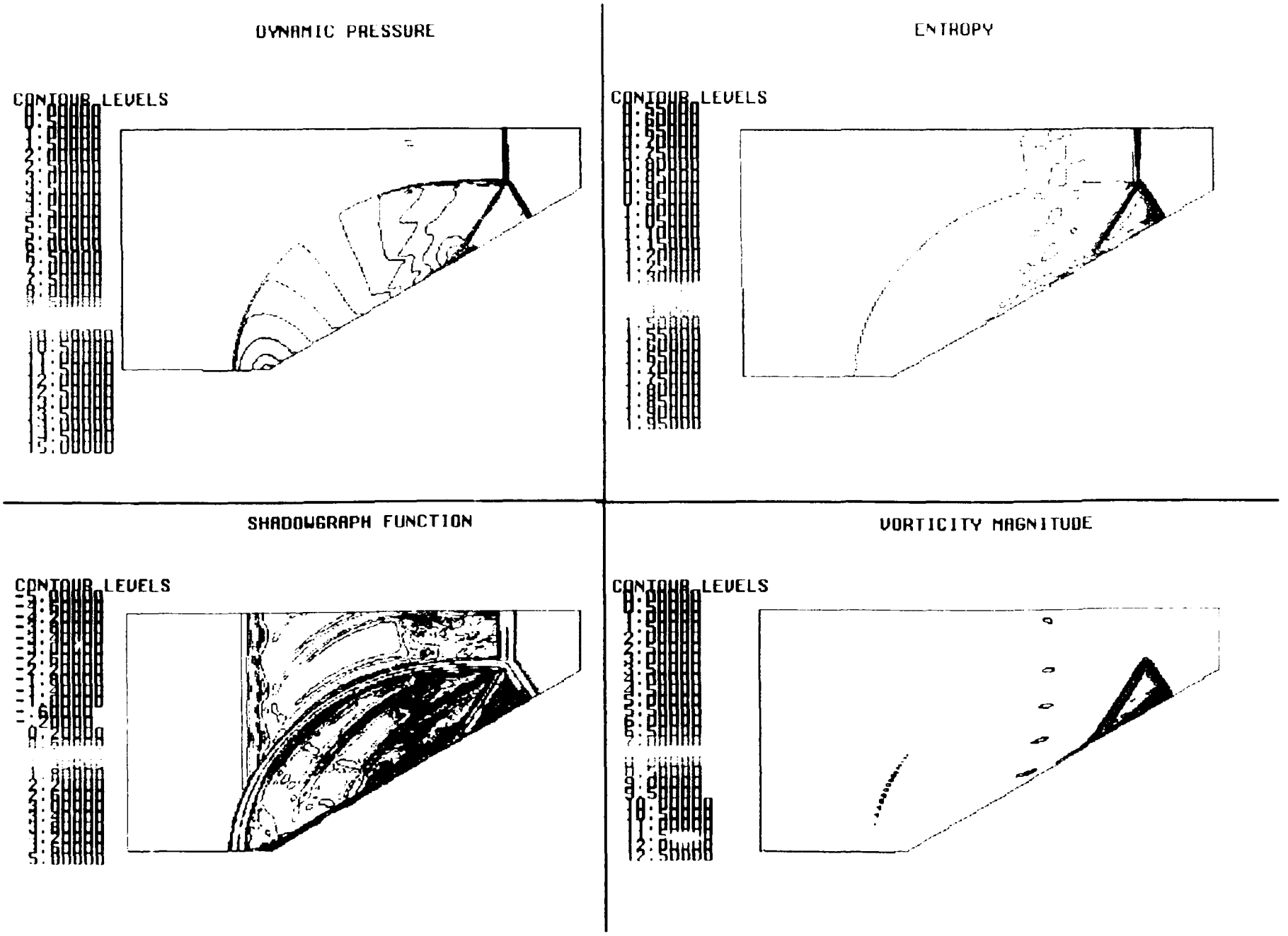

Figure 9. Dynamic Pressure, Entropy, Shadowgraph Function, and Vorticity Magnitude Contours, $M_I = 2.12$, 98×25 grid, 30 Degree Wedge

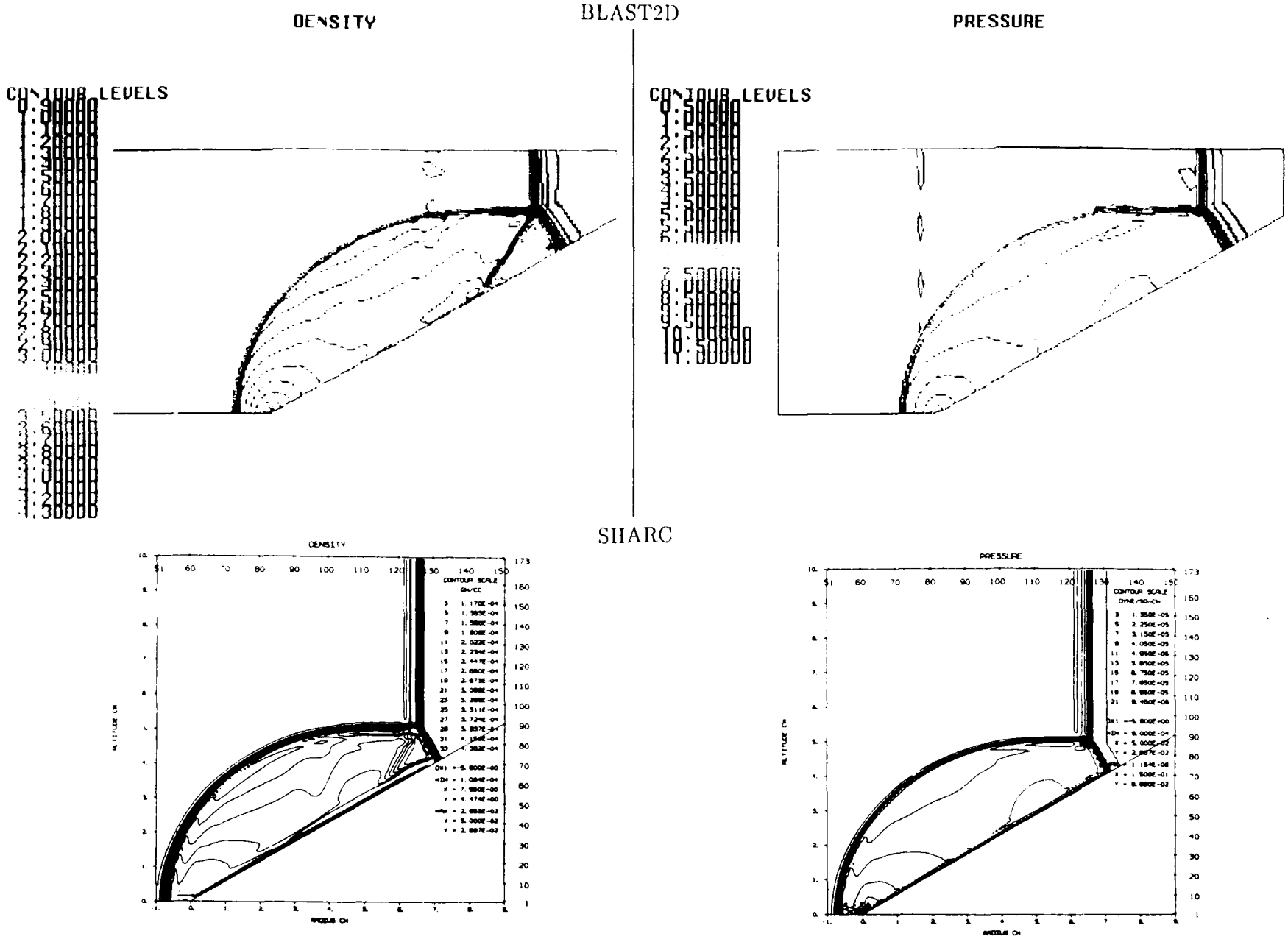

Figure 10. Density,Pressure Contour Plot Comparisons between BLAST2D and SHARC

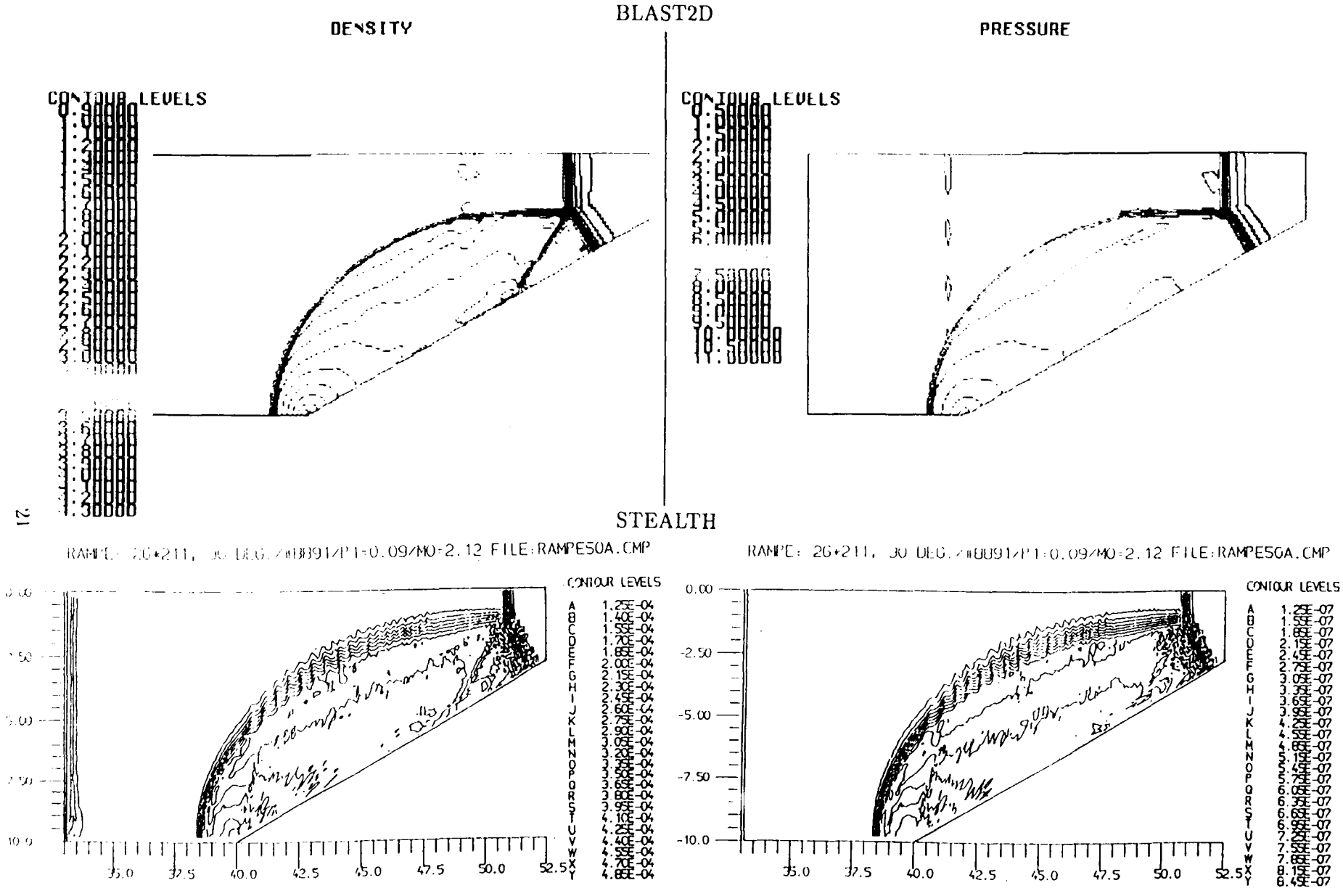

Figure 11. Density,Pressure Contour Plot Comparisons between BLAST2D and STEALTH

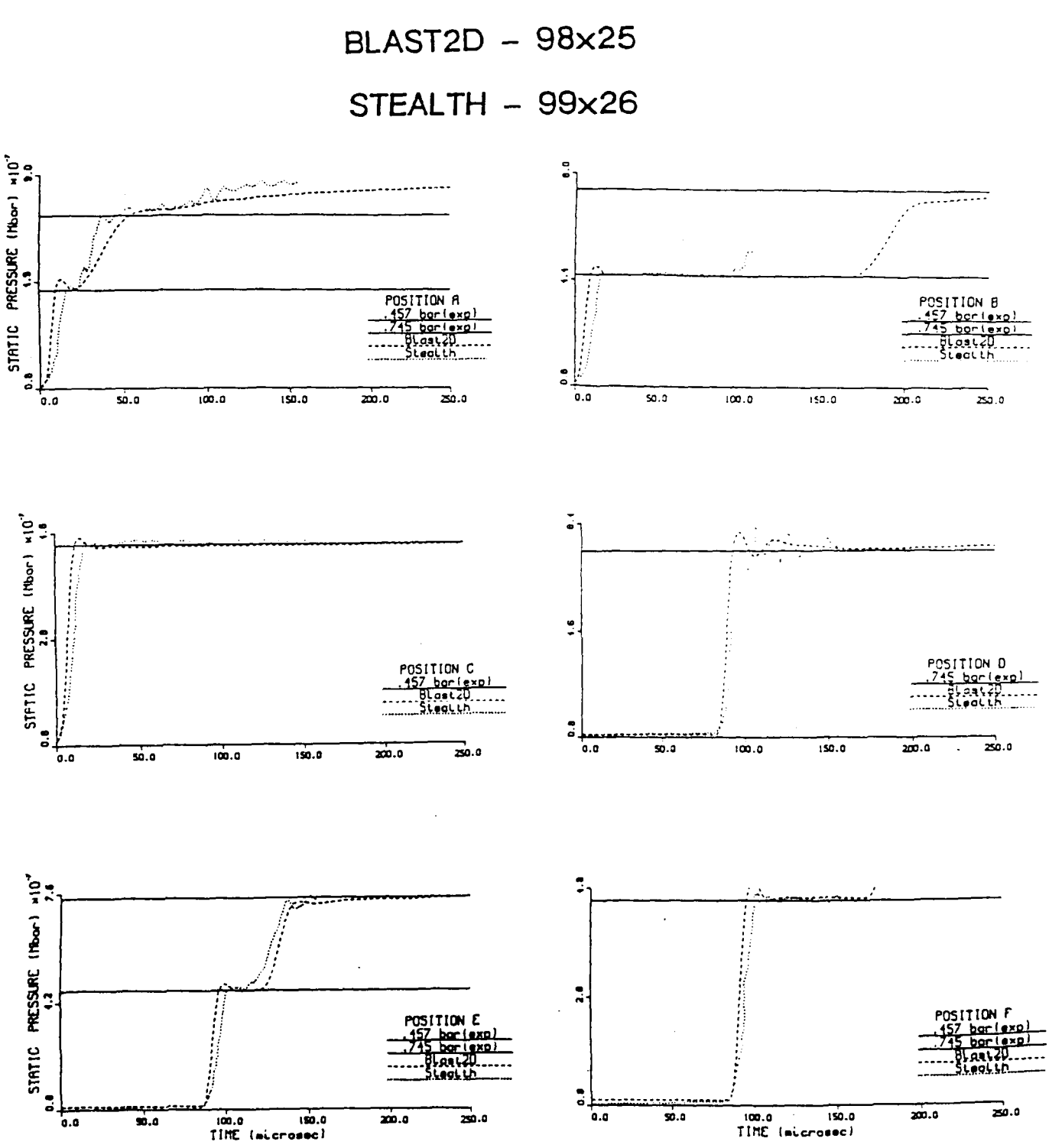

Figure 12. Pressure versus Time Histories, Positions A-F, BLAST2D 98×25 Grid, STEALTH 99×26 Grid

BLAST2D - 189x172

STEALTH - 99x26

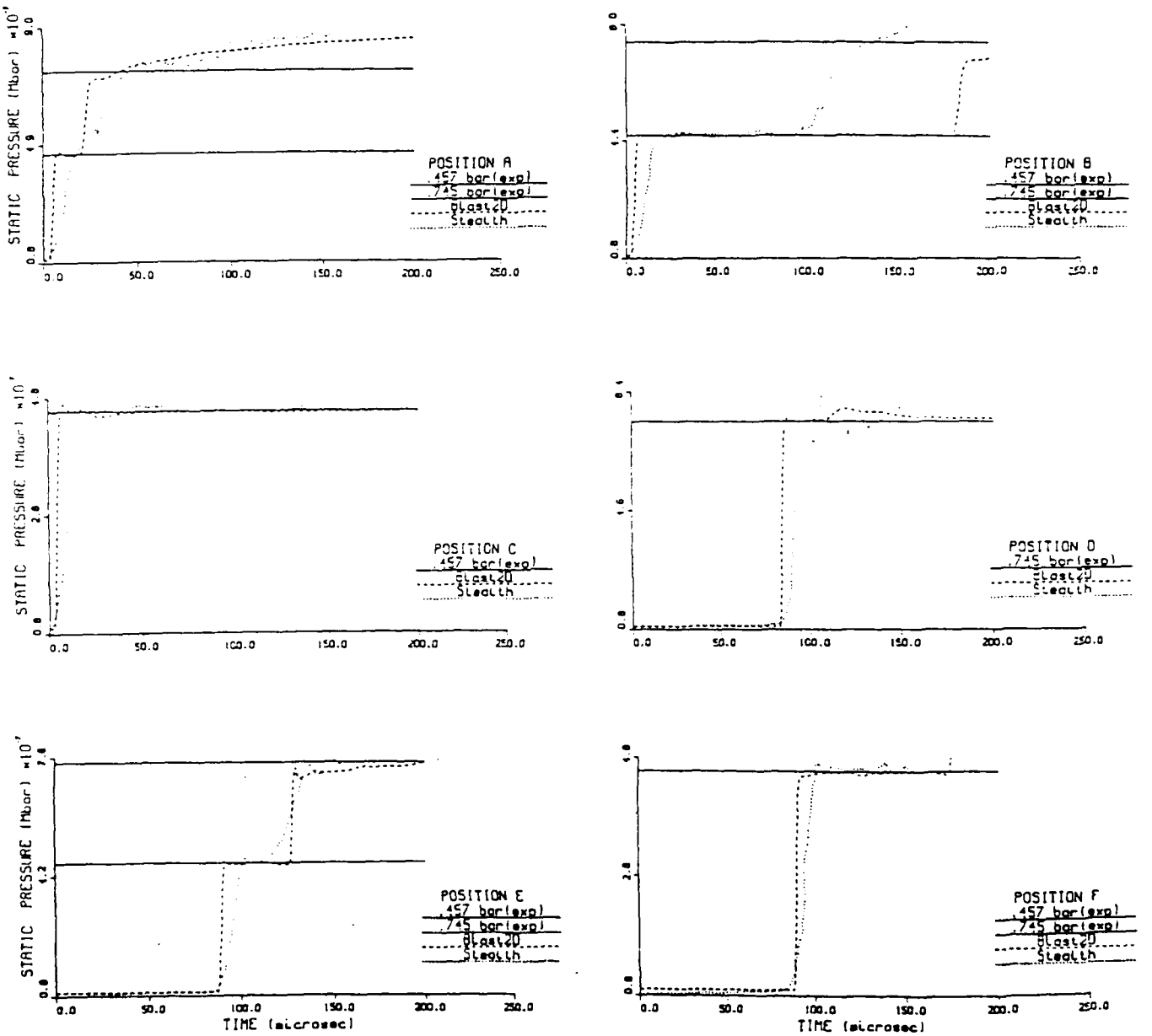

Figure 13. Pressure versus Time Histories, Positions A-F, BLAST2D 189×172 Grid, STEALTH 99×26 Grid

BLAST2D – 189x172

SHARC – 189x172

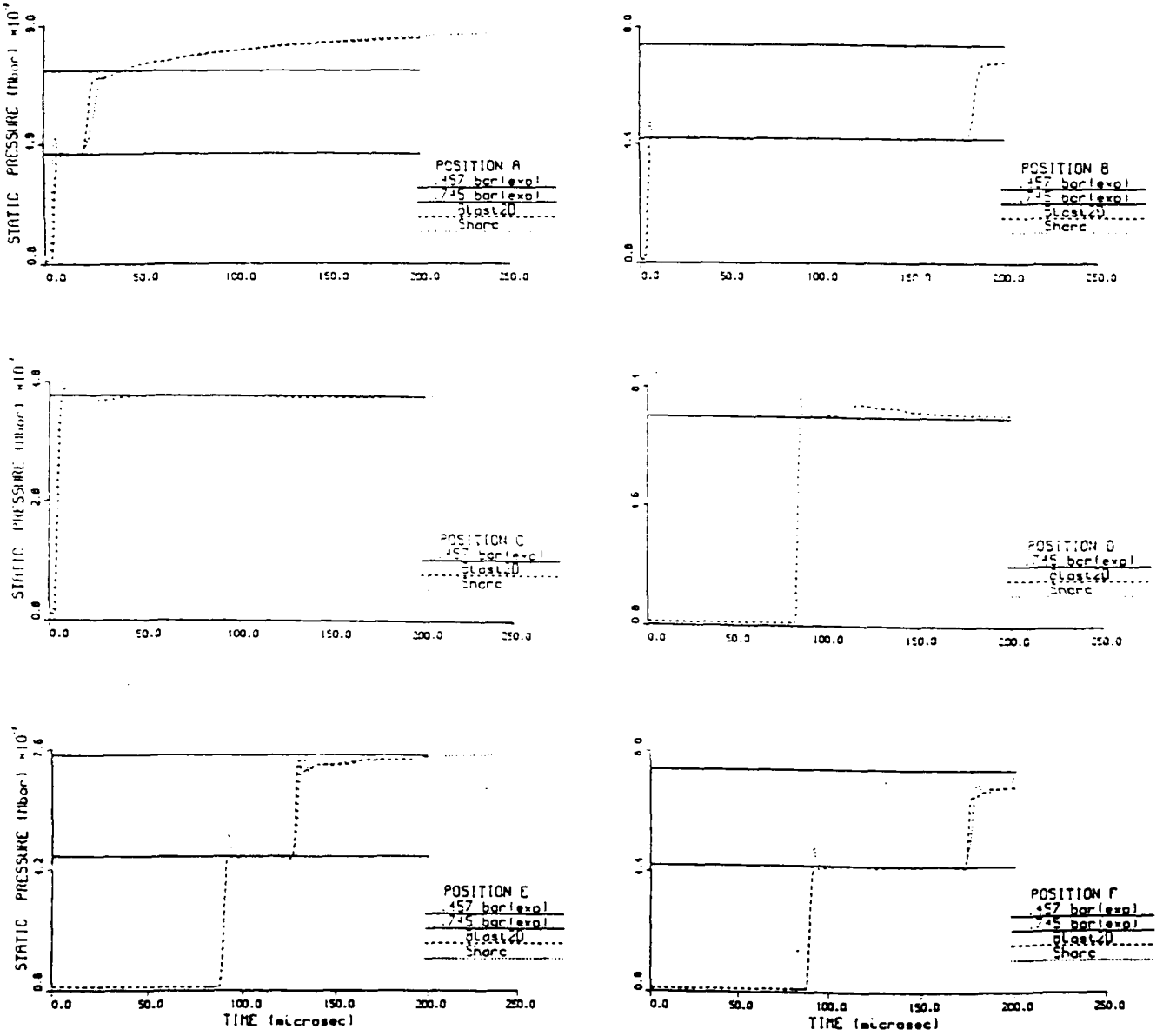

Figure 14. Pressure versus Time Histories, Positions A-F, BLAST2D 189×172 Grid, SHARC 189×172 Grid

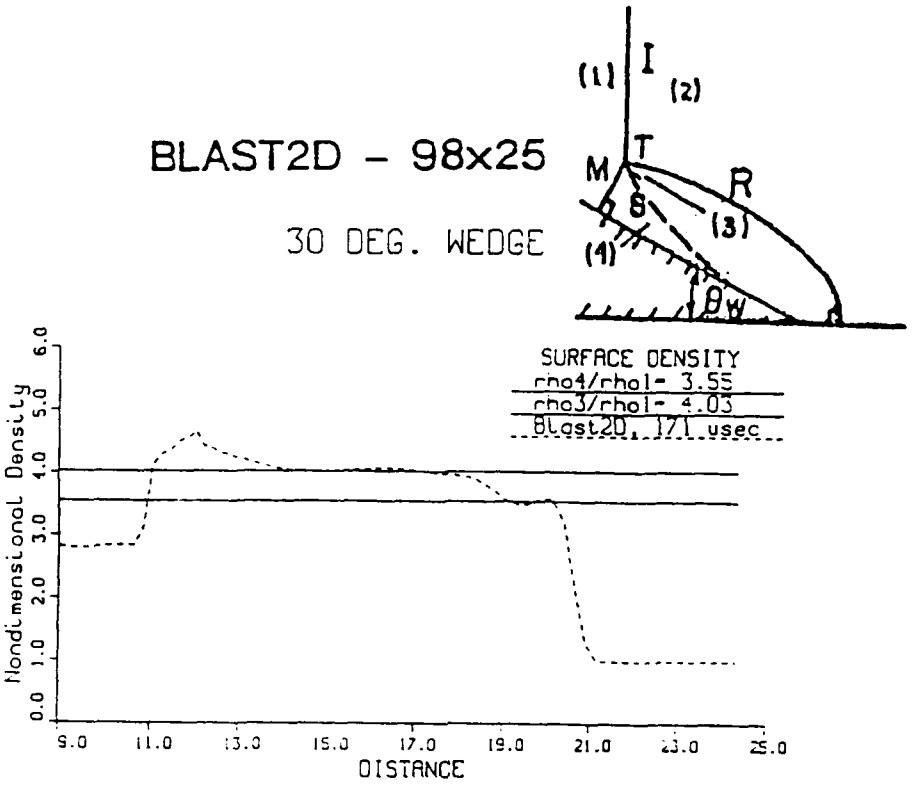

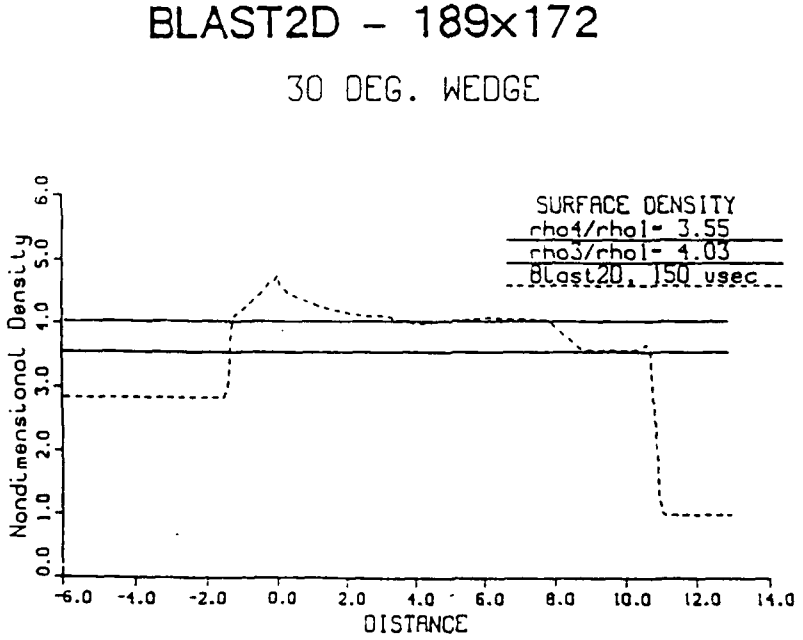

Figure 15. Surface Density Plots - BLAST2D with 98×25 Grid and 189×172 Grid

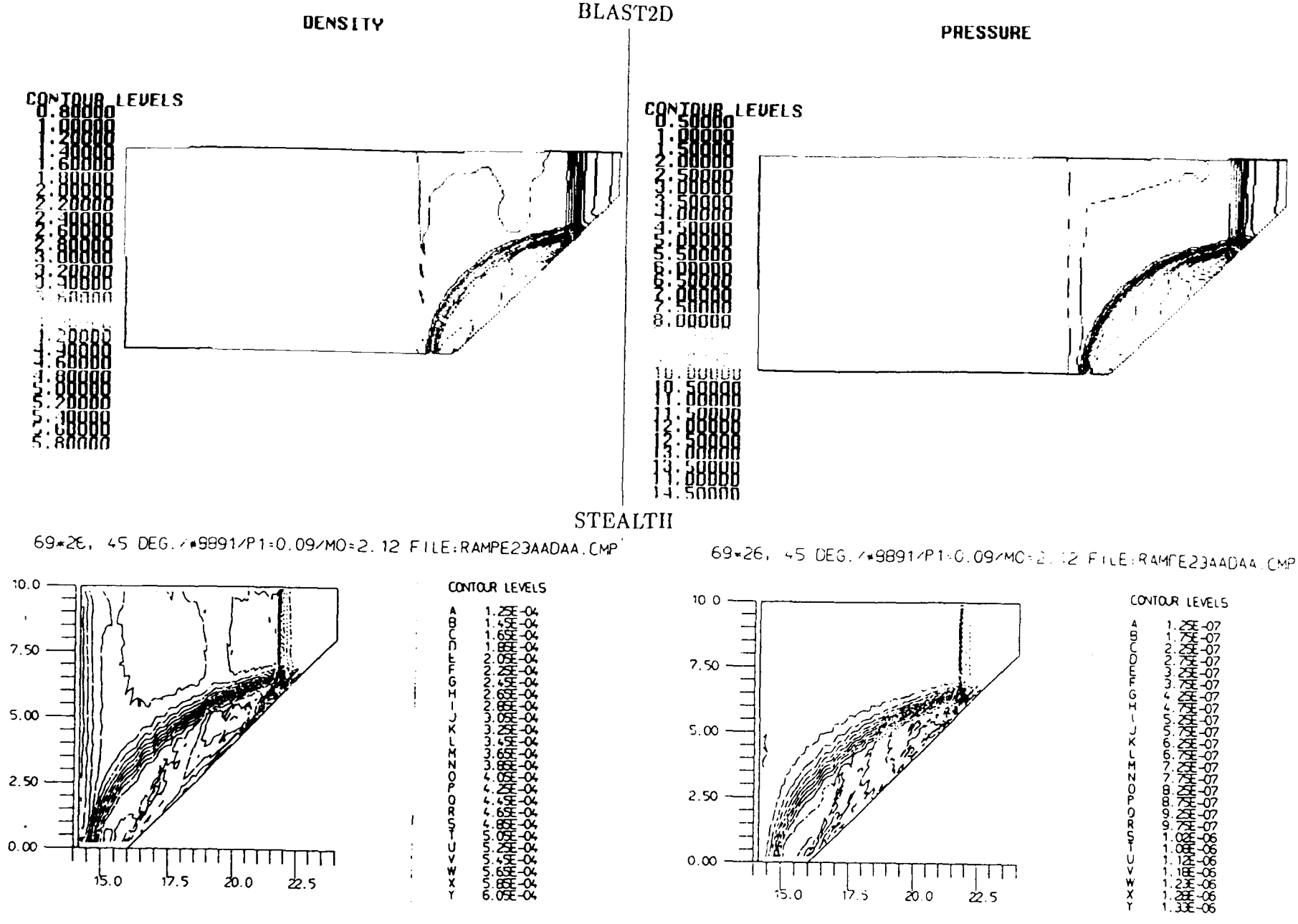

Figure 16. Density and Pressure Contour Comparisons between BLAST2D and STEALTH, $M_I = 2.12$, 68×25 Grid, 45 Degree Wedge

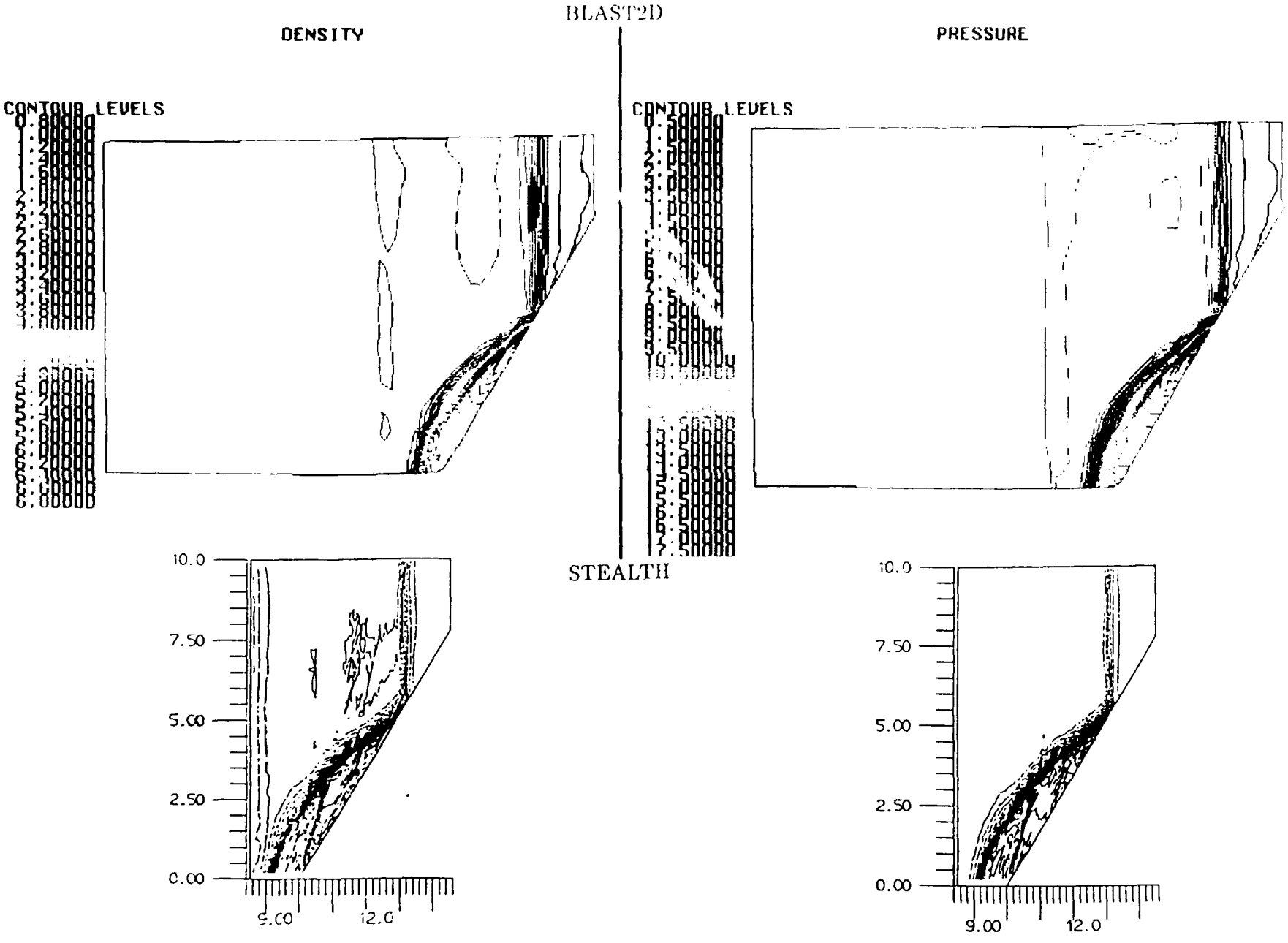

Figure 17. Density and Pressure Contour Comparisons between BLAST2D and STEALTH, $M_I = 2.12$, 46×25 Grid, 60 Degree Wedge

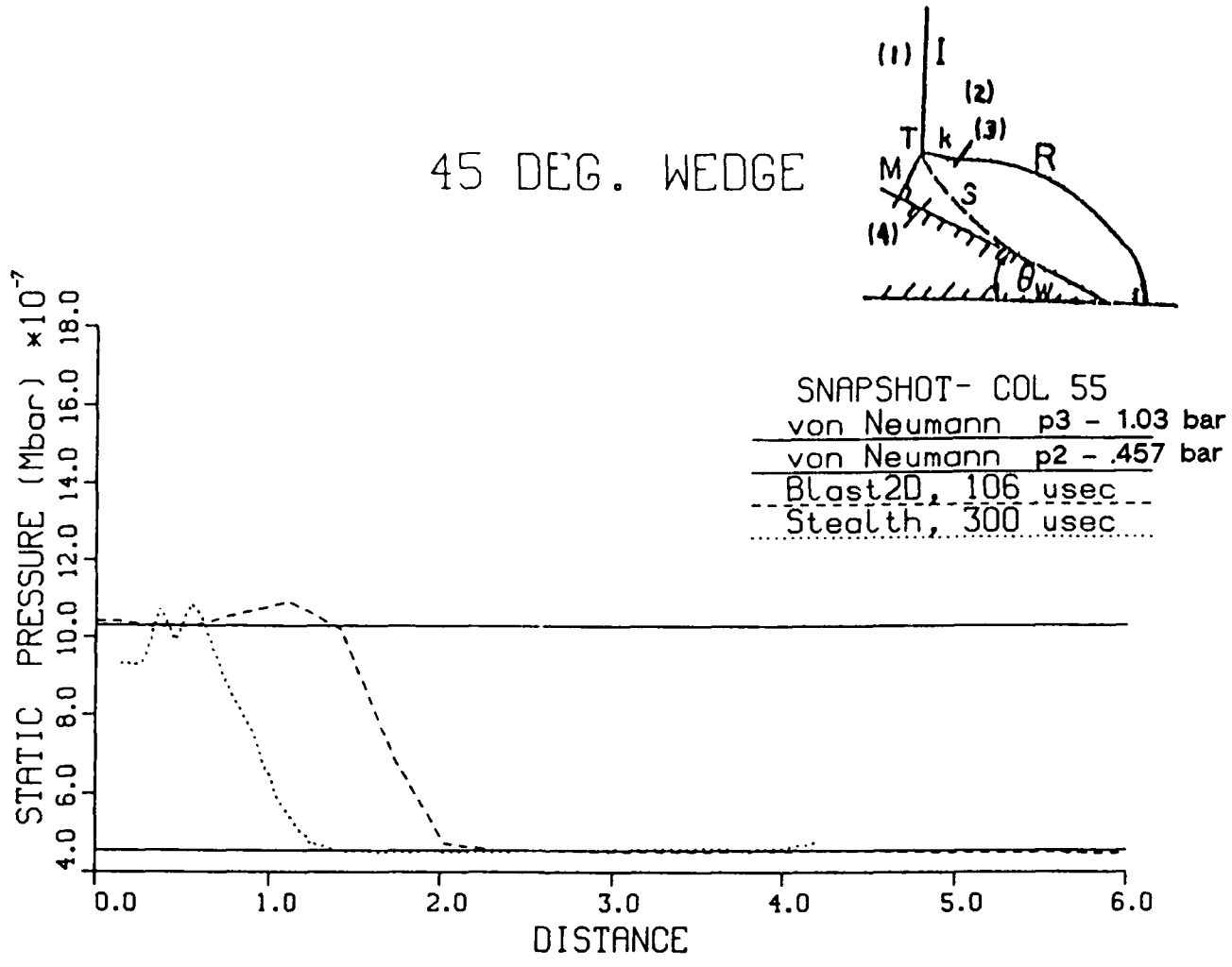

Figure 18. Snapshot of Column 55 Pressure Comparison, BLAST2D and STEALTH, M_I =2.12, 45 Degree Wedge

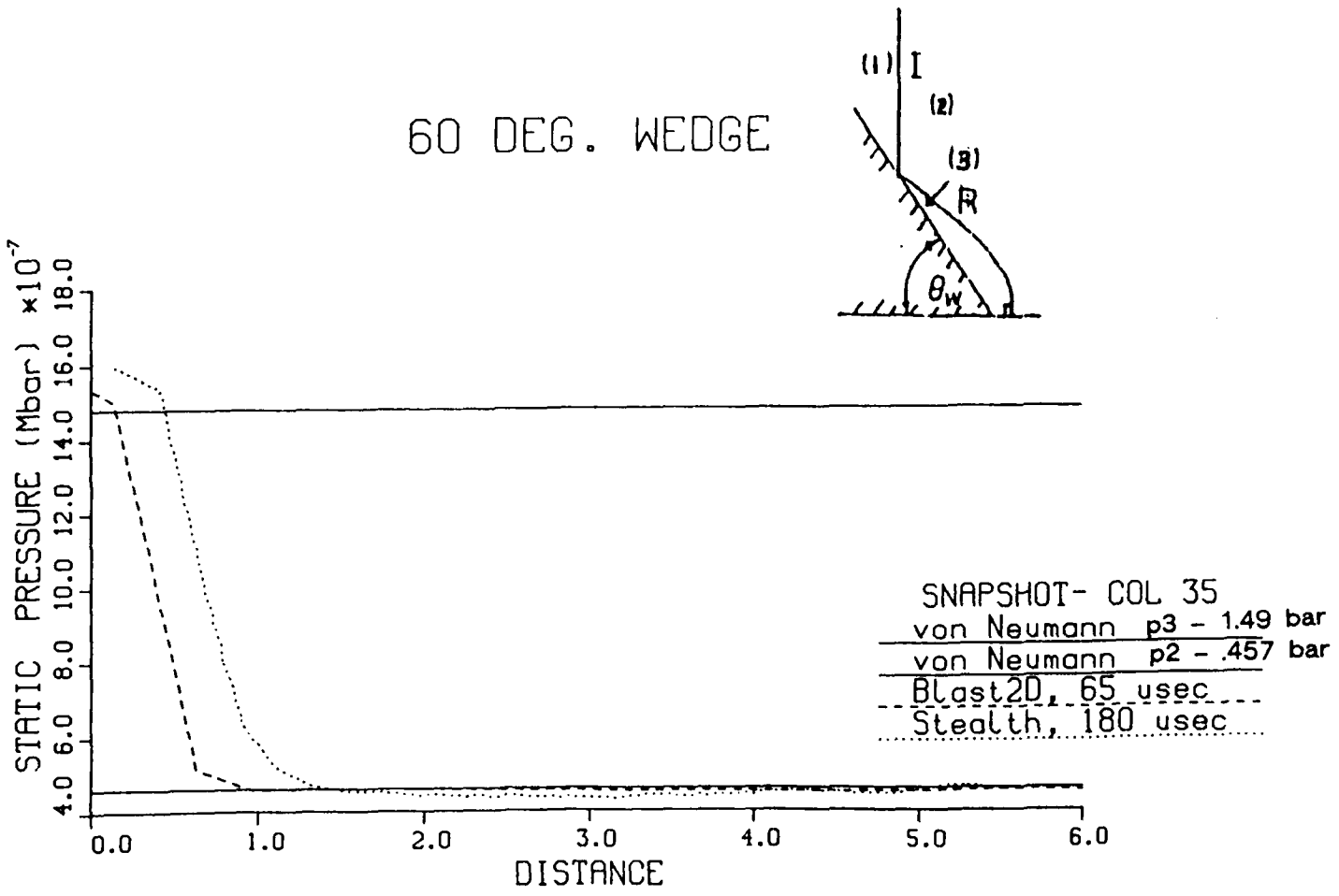

Figure 19. Snapshot of Column 35 Pressure Comparison, BLAST2D and STEALTH, M_I =2.12, 60 Degree Wedge

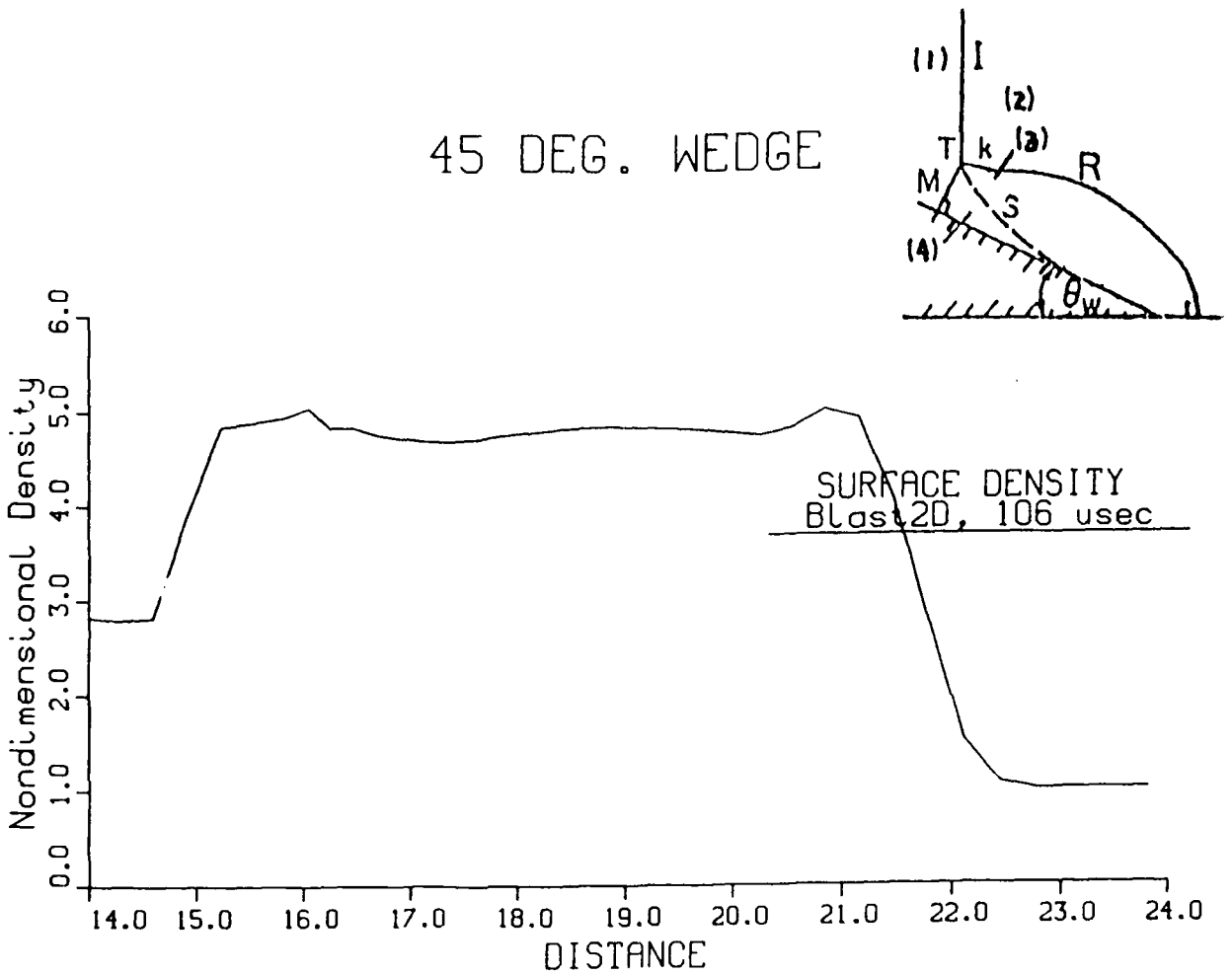

Figure 20. Surface Density Plot, BLAST2D, 45 Degree Wedge

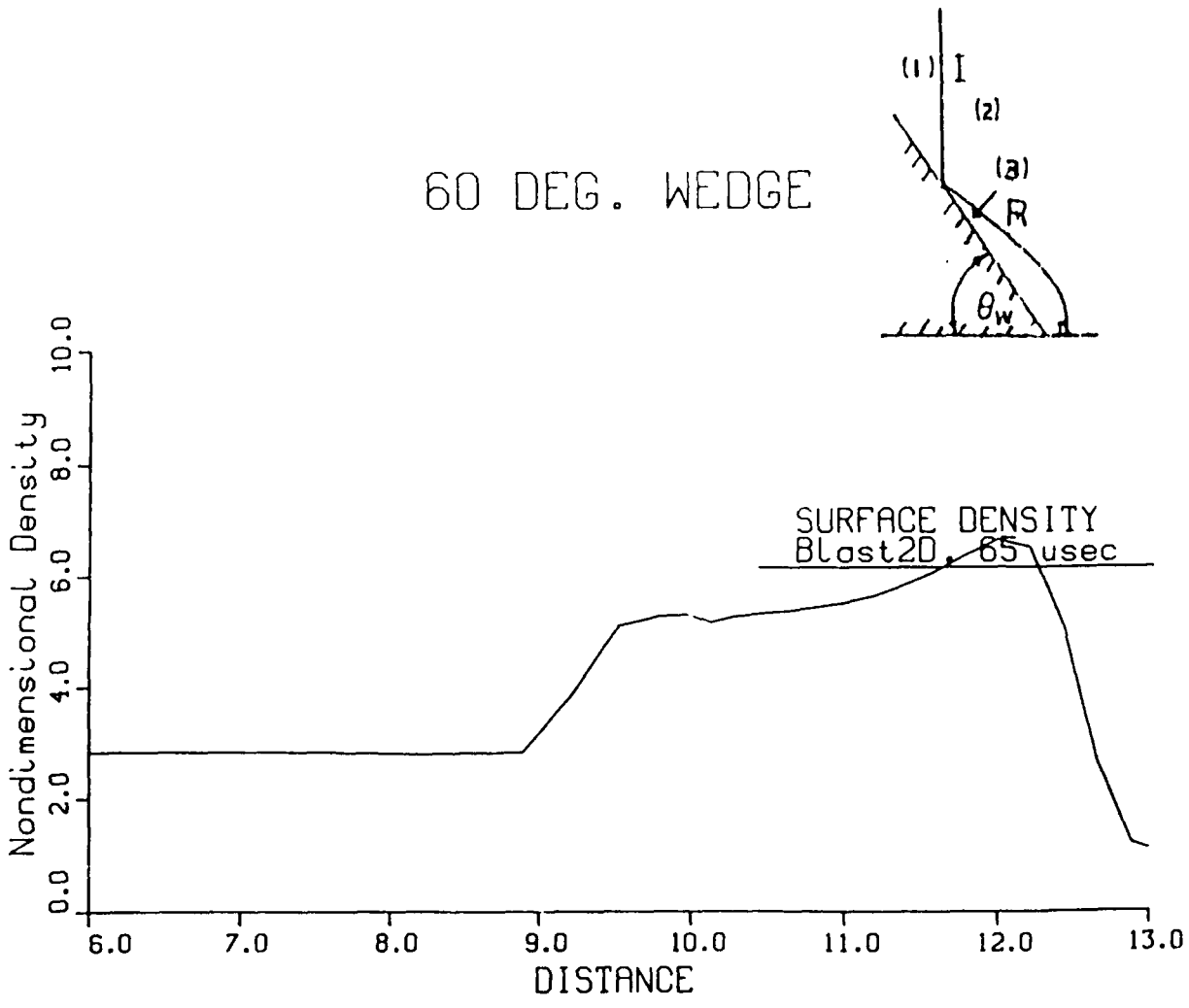

Figure 21. Surface Density Plot, BLAST2D, 60 Degree Wedge

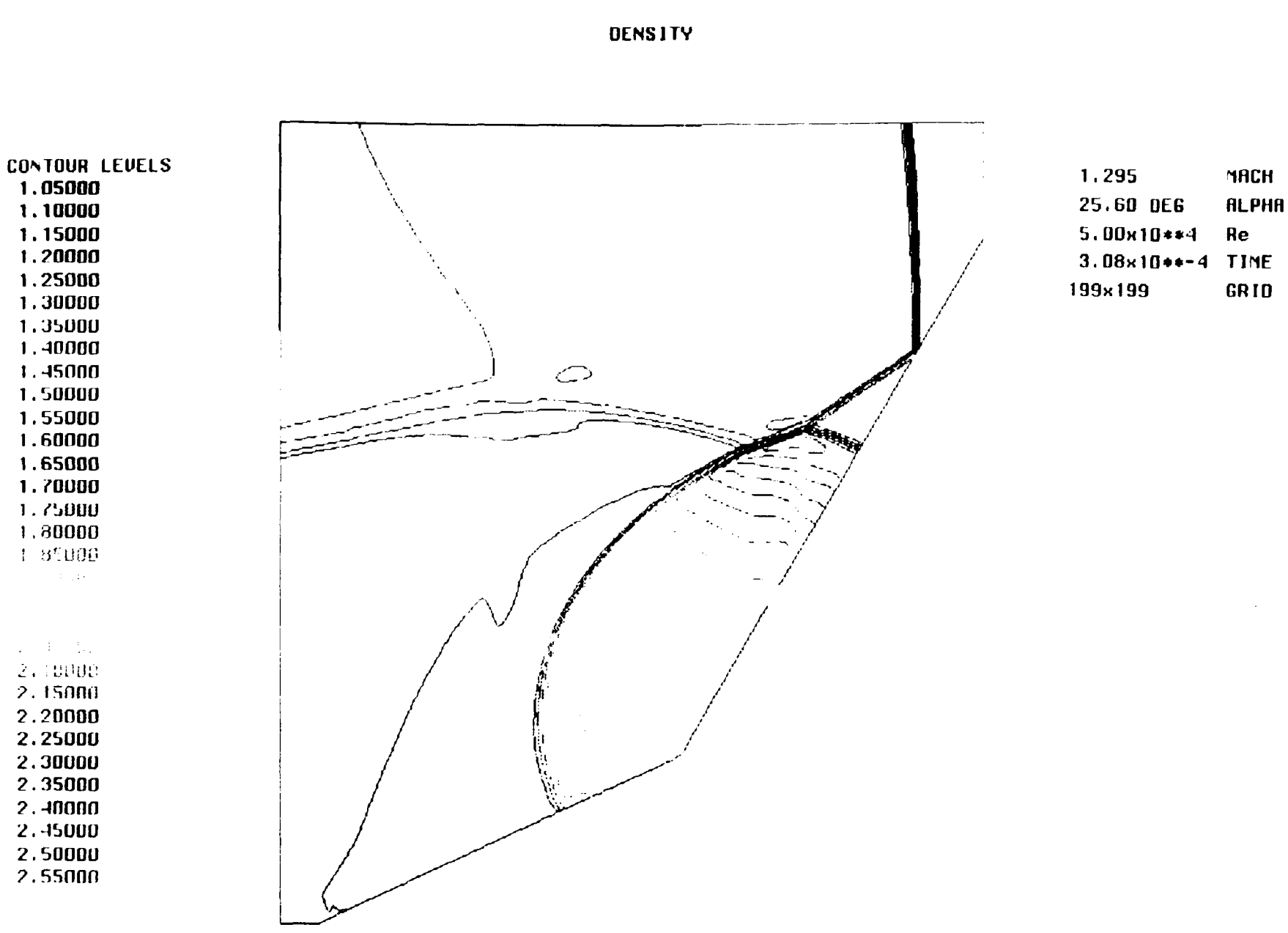

Figure 22. Density Contour Plot, 25 and 60 Degree Double Wedge

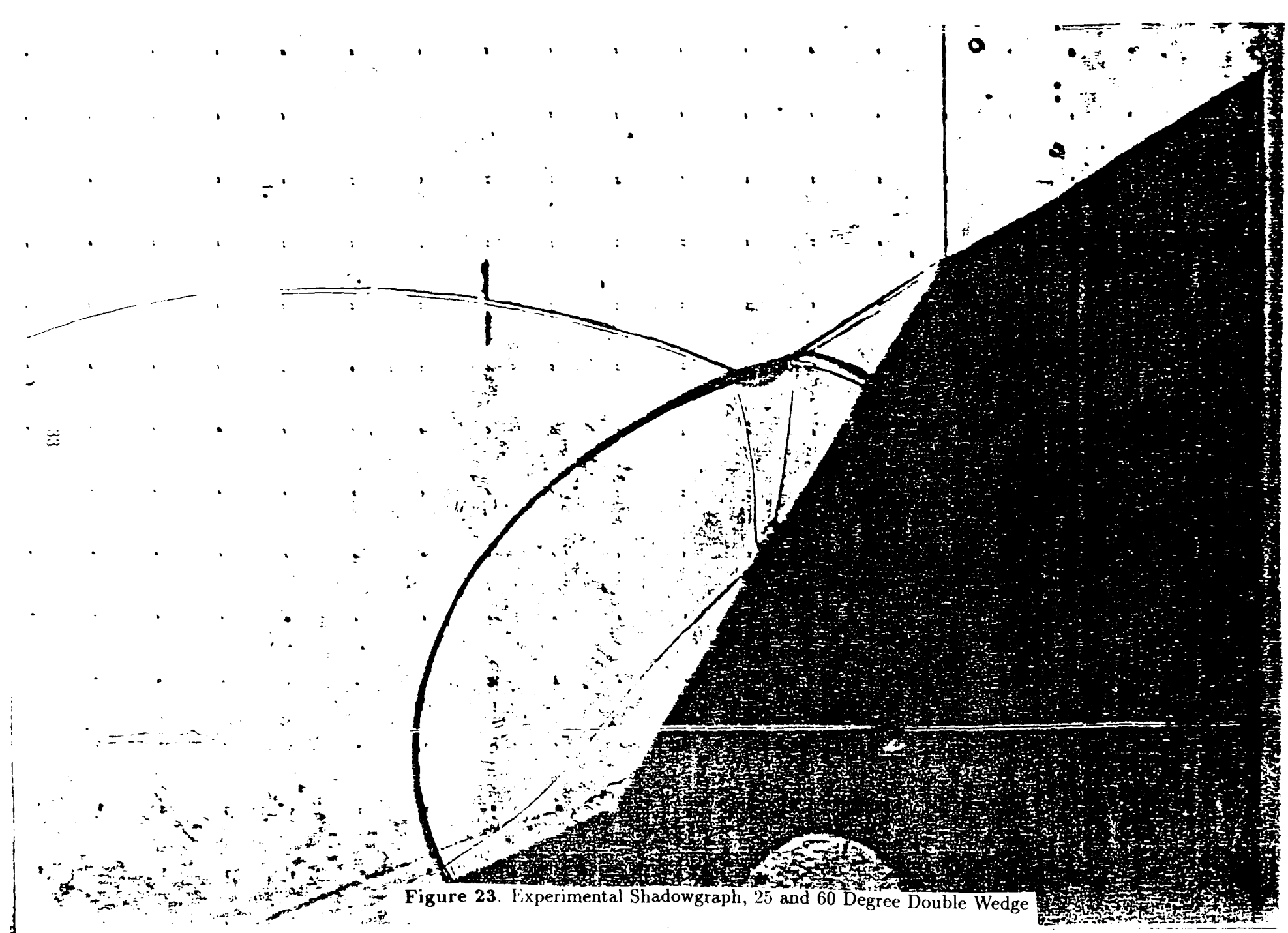

Figure 23. Experimental Shadowgraph, 25 and 60 Degree Double Wedge

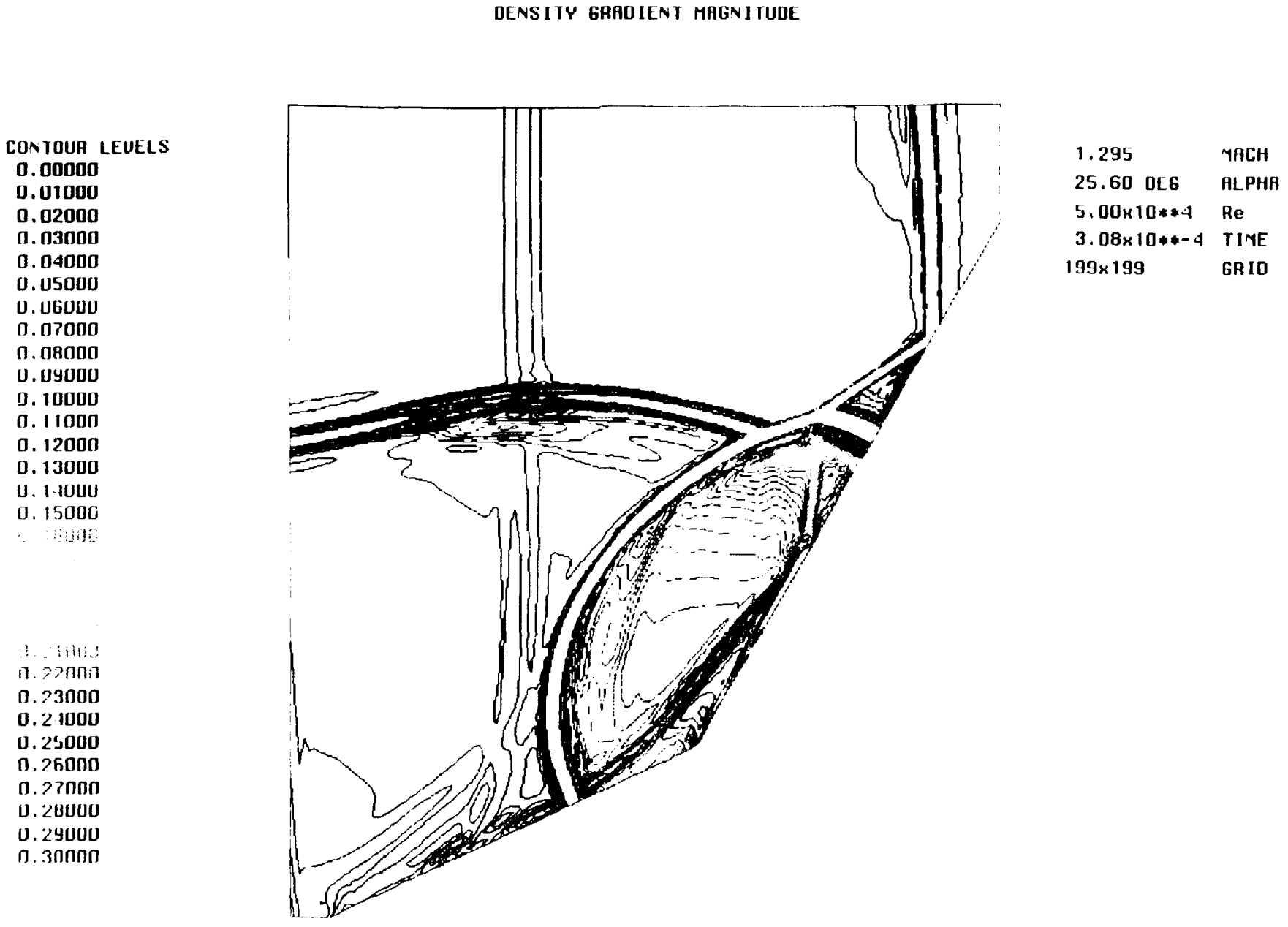

Figure 24. Density Gradient Magnitude Contour Plot, 25 and 60 Degree Double Wedge

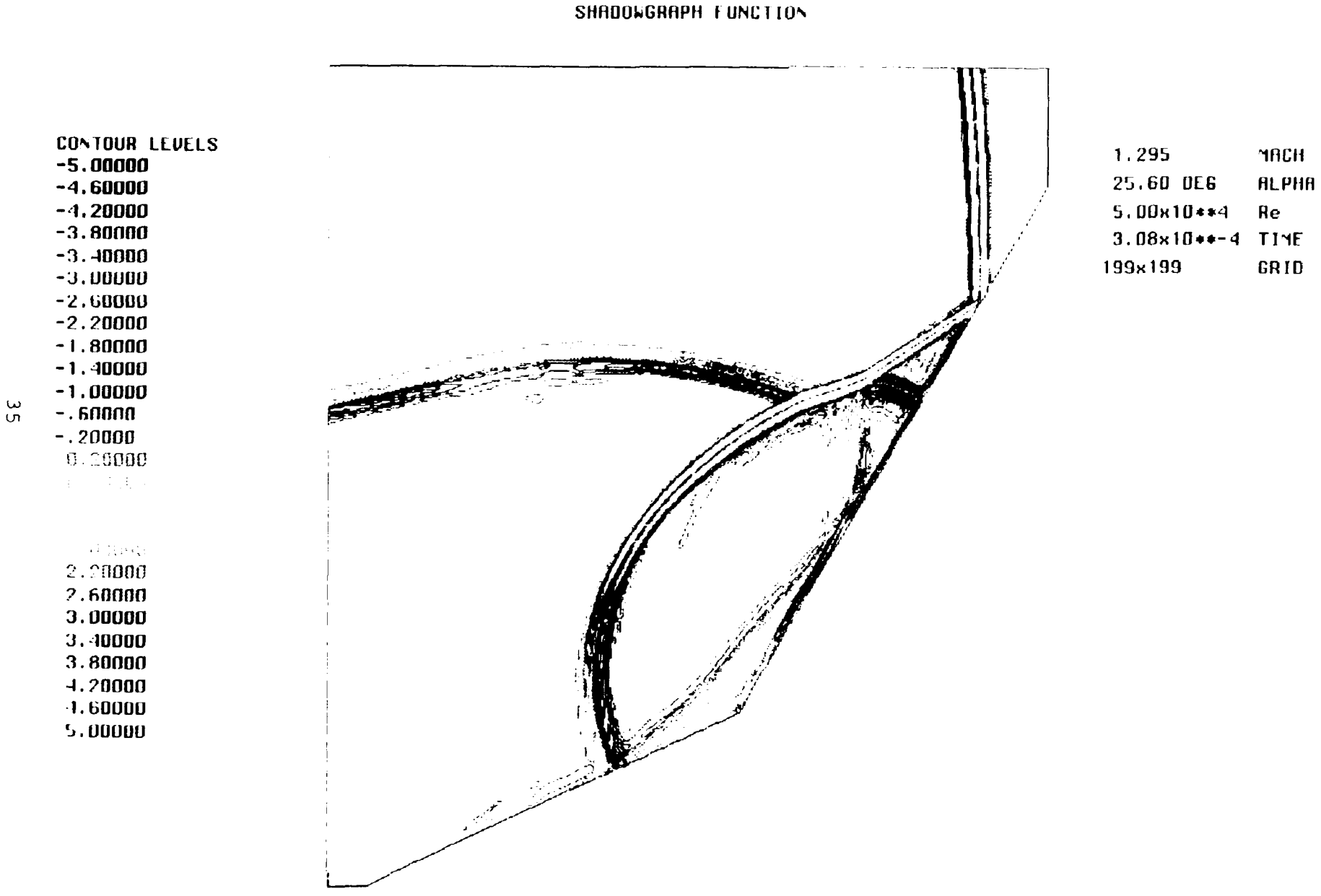

Figure 25. Shadowgraph Function Contour Plot, 25 and 60 Degree Double Wedge

INTENTIONALLY LEFT BLANK.

LIST OF REFERENCES

1. H. M. Glas, P. Colella, I. I. Glass, and R. L. Deschambault, "A Detailed Numerical, Graphical, and Experimental Study of Oblique Shock Wave Reflections", UTIAS Report No. 285, CN ISSN 0082-5255, Institute for Aerospace Studies, University of Toronto, August 1986.

2. M. Shirouzu and I. I. Glass, "An Assessment of Recent Results on Pseudo-Stationary Oblique-Shock-Wave Reflections", Presented at the 4th Mach Reflection Symposium, Tokyo and Sendai, June 18-22, 1984.

3. R. L. Deschambault and I. I. Glass, "An Update on Non-stationary Oblique Shock-wave Reflections: Actual Isopycnics and Numerical Experiments", Journal of Fluid Mechanics, vol. 131, 1983., pp. 27-57.

4. G. D. Lock and J. M. Dewey, "An Experimental Investigation of the Sonic Criterion for Transition from Regular to Mach Reflection of Weak Shock Waves", Experiments in Fluids, vol. 7, 1989, pp. 289-292.

5. K. Takayama, and G. Ben-Dor, "The Inverse Mach Reflection", AIAA Journal, vol.23, No.12, December 1985, pp 1853-1859.

6. G. Ben-Dor, J. M. Dewey, and O. Ingra, "Analytical Investigation of Reflection of a Regular or Mach Reflection over a Secondary Wedge," Final Report- Contract DAJA 45-86-C-0038, November 1,1986 - October 30,1987.

7. D. F. Dawson, C. E. Needhan, K. Hibray, H. J. Happ III, "Hydrodynamic Simulation of Double Wedge Reflection", Presented by Prof. John Dewey, University of Victoria, at The 16th International Symposium on Shock Tubes and Waves, July 26 - July 30, 1987.

8. S. Hikida, R. L. Bell, C. E. Needham, "The SHARC Codes: Documentation and Sample Problems. Volume I: Inviscid Fluid Dynamics", SSS-R-89-9878, S-Cubed, A Division of Maxwell Laboratories, Inc., Albuquerque, NM, September 1988.

9. "E STEALTH- A Lagrange Explicit Finite Difference Code for Solids, Structural, and Thermodynamic Analysis", Science Applications International Corporation, San Leandro, California 94577.

10. D.M. Hisley, and G.A. Molvik, "Axisymmetric Calculations for the Large Blast/Thermal Simulator (LB/TS) Shock Tube Configuration", BRL-TR-2935, US Army Ballistic Research Laboratory, Aberdeen Proving Ground, Maryland, 21005, September 1988.

11. G. A. Molvik, "Computation of Viscous Blast Wave Solutions with an Upwind Finite Volume Method", AIAA Paper 87-1290, Honolulu, HA, June 1987.

12. P. L. Roe, "Approximate Riemann Solvers, Parameter Vectors, and Difference Schemes", Journal of Computational Physics, Vol. 43, 1981, pp. 357-372.

13. S. R. Chakravarthy, "A New Class of High Accuracy TVD Schemes for Hyperbolic Conservation Laws", AIAA Paper, 85-0363, Reno, NV, Jan. 1985.

14. M. M. Rai, "An Implicit Form for the Osher Upwind Scheme", AIAA Paper 84-0088, Reno, NV, Jan. 1984.

15. Heilig, W., Private Communication, September 8, 1989.

16. R. E. Lottero, and J. D. Wortman, "Evaluation of the HULL and SHARC Hydrocodes in Simulating the Reflection of a Mach 2.12 Non-Decaying Shock on Wedges of Various Angles", Brl Technical Report, to be published.

APPENDIX A: Function Definitions

INTENTIONALLY LEFT BLANK.

p - static pressure

ρ - density

u - x component velocity

v - y component velocity

C_v - specific heat at constant volume

C_p - specific heat at constant pressure

Velocity magnitude

$$V = \sqrt{u^2 + v^2} \tag{A-1}$$

Speed of sound

$$a = \sqrt{\frac{\gamma p}{\rho}} \tag{A-2}$$

Mach number

$$M = \frac{V}{a} \tag{A-3}$$

Dynamic pressure

$$Q = 1/2\rho(u^2 + v^2) \tag{A-4}$$

Entropy

$$S = C_v ln \frac{p}{p_\infty} + C_p ln \frac{\rho_\infty}{\rho} \tag{A-5}$$

Shadowgraph function

$$f = \frac{\partial^2 \rho}{\partial x^2} + \frac{\partial^2 \rho}{\partial y^2} \tag{A-6}$$

Vorticity magnitude

$$\Omega = \frac{dv}{dx} - \frac{du}{dy} \tag{A-7}$$

INTENTIONALLY LEFT BLANK.

No of Copies	Organization
1	Office of the Secretary of Defense OUSD(A) Director, Live Fire Testing ATTN: James F. O'Bryon Washington, DC 20301-3110
2	Administrator Defense Technical Info Center ATTN: DTIC-DDA Cameron Station Alexandria, VA 22304-6145
1	HQDA (SARD-TR) WASH DC 20310-0001
1	Commander US Army Materiel Command ATTN: AMCDRA-ST 5001 Eisenhower Avenue Alexandria, VA 22333-0001
1	Commander US Army Laboratory Command ATTN: AMSLC-DL Adelphi, MD 20783-1145
2	Commander US Army, ARDEC ATTN: SMCAR-IMI-I Picatinny Arsenal, NJ 07806-5000
2	Commander US Army, ARDEC ATTN: SMCAR-TDC Picatinny Arsenal, NJ 07806-5000
1	Director Benet Weapons Laboratory US Army, ARDEC ATTN: SMCAR-CCB-TL Watervliet, NY 12189-4050
1	Commander US Army Armament, Munitions and Chemical Command ATTN: SMCAR-ESP-L Rock Island, IL 61299-5000
1	Commander US Army Aviation Systems Command ATTN: AMSAV-DACL 4300 Goodfellow Blvd. St. Louis, MO 63120-1798

No of Copies	Organization
1	Director US Army Aviation Research and Technology Activity ATTN: SAVRT-R (Library) M/S 219-3 Ames Research Center Moffett Field, CA 94035-1000
1	Commander US Army Missile Command ATTN: AMSMI-RD-CS-R (DOC) Redstone Arsenal, AL 35898-5010
1	Commander US Army Tank-Automotive Command ATTN: AMSTA-TSL (Technical Library) Warren, MI 48397-5000
1	Director US Army TRADOC Analysis Command ATTN: ATAA-SL White Sands Missile Range, NM 88002-5502
(Class. only) 1	Commandant US Army Infantry School ATTN: ATSH-CD (Security Mgr.) Fort Benning, GA 31905-5660
(Unclass. only) 1	Commandant US Army Infantry School ATTN: ATSH-CD-CSO-OR Fort Benning, GA 31905-5660
1	Air Force Armament Laboratory ATTN: AFATL/DLODL Eglin AFB, FL 32542-5000
	Aberdeen Proving Ground
2	Dir, USAMSAA ATTN: AMXSY-D AMXSY-MP, H. Cohen
1	Cdr, USATECOM ATTN: AMSTE-TD
3	Cdr, CRDEC, AMCCOM ATTN: SMCCR-RSP-A SMCCR-MU SMCCR-MSI
1	Dir, VLAMO ATTN: AMSLC-VL-D

DISTRIBUTION LIST

No. of Copies	Organization
1	Director of Defense Research & Engineering ATTN: DD/TWP Washington, DC 20301
1	Assistant Secretary of Defense (Atomic Energy) ATTN: Document Control Washington, DC 20301
1	Chairman Joint Chiefs of Staff ATTN: J-5 (R&D Div) Washington, DC 20301
2	Deputy Chief of Staff for Operations and Plans ATTN: Technical Library Director of Chemical and Nuclear Operations Department of the Army Washington, DC 20310
1	Director Defense Advanced Research Projects Agency ATTN: Tech Lib 1400 Wilson Boulevard Arlington, VA 22209
2	Director Federal Emergency Management Agency ATTN: Public Relations Office Technical Library Washington, DC 20472
1	Director Defense Intelligence Agency ATTN: DT-2/Wpns & Sys Div Washington, DC 20301
1	Director National Security Agency ATTN: R15 (E. F. Butala) Ft. George G. Meade, MD 20755
7	Director Defense Nuclear Agency ATTN: CSTI (Tech Lib) DDIR DFSP (Ullrich) NANS OPNA SPSD (Goering/Rohr) TDTR (Kennedy/Hrinishin) Washington, DC 20305
3	Commander Field Command, DNA ATTN: FCPR FCTMOF NMHE/CDR Lund Kirtland AFB, NM 87115
10	Central Intelligence Agency DIR/DB/Standard ATTN: GE-47 HQ Washington, DC 20505
4	Director US Army Harry Diamond Labs ATTN: SLCHD-NW-RA (L. Belliveau) SLCHD-NW-P (Ms. Abe/Mr. Corrigan) SLCHD-TA-L (Tech Lib) 2800 Powder Mill Road Adelphi, MD 20783-1197
2	Commander US Army CECOM ATTN: AMSEL-RD AMSEL-RO-TPPO-P Fort Monmouth, NJ 07703-5301
1	Commander, USACECOM R&D Technical Library ATTN: ASQNC-ELC-I-T Myer Center Fort Monmouth, NJ 07703-5301
1	Director US Army Missile and Space Intelligence Center ATTN: AIAMS-YDL Redstone Arsenal, AL 35898-5500

DISTRIBUTION LIST

No. of Copies	Organization
1	Commander US Army Foreign Science and Technology Center ATTN: Research & Data Branch 220 7th Street , NE. Charlottesville, VA 22901
1	Director US Army TRAC - Ft. Lee ATTN: ATRC-L (Mr. Cameron) Fort Lee, VA 23801-6140
1	Director US Army Materials Technology Laboratory ATTN: SMCMT-ATL Watertown, MA 02172-0001
1	Commander US Army Strategic Defense Command ATTN: CSSD-H-MPL (Tech Lib) CSSD-H-XM (Dr. Davies) P.O. Box 1500 Huntsville, AL 35807
2	Commander US Army Natick Research and Development Center ATTN: AMDNA-D (Dr. D. Sieling) STRNC-UE (J. Calligeros) Natick, MA 01762
1	Commander US Army Engineer Division ATTN: HNDED-FD P.O. Box 1500 Huntsville, AL 35807
3	Commander US Army Corps of Engineers Waterways Experiment Station ATTN: CAWES-SS-R (J. Watt) CAWES-SE-R (J. Ingram) CAWES-TL (Tech Lib) P.O. Box 631 Vicksburg, MS 39180-0631
1	Commander US Army Research Office ATTN: SLCRO-D P.O. Box 12211 Research Triangle Park, NC 27709-2211
3	Commander US Army Nuclear & Chemical Agency ATTN: ACTA-NAW MCNA-WE Tech. Lib. 7500 Backlick Rd, Bldg. 2073 Springfield, VA 22150
1	Director HQ, TRAC RPD ATTN: ATRC-RPR (Mr. Radda) Fort Monroe, VA 23651-5143
1	Director TRAC-WSMR ATTN: ATRC-WC (Mr. Kirby) White Sands Missile Range, NM 88002-5502
1	Director US Army TRAC ATTN: ATRC Fort Leavenworth, KS 66027-5200
1	Commander US Army Test & Evaluation Command Nuclear Effects Laboratory ATTN: STEWS-TE-NO (Dr. J.L. Meason) P.O. Box 477 White Sands Missile Range, NM 88002
2	Director Joint Strategic Target Planning Staff JCS ATTN: JLTW TPTP Offut AFB Omaha, NB 68113

DISTRIBUTION LIST

No. of Copies	Organization
1	Commandant Interservice Nuclear Weapons School ATTN: Technical Library Kirtland AFB, NM 87115
2	Chief of Naval Operations ATTN: OP-03EG OP-985F Department of the Navy Washington, DC 20350
1	Chief of Naval Research ATTN: N. Perrone Department of the Navy Arlington, VA 22217
1	Director Strategic Systems Projects Office ATTN: NSP-43, Tech Library Department of the Navy Washington, DC 20360
1	Commander Naval Electronic Systems Command ATTN: PME 117-21A Washington, DC 20360
1	Commander Naval Facilities Engineering Command ATTN: Technical Library Washington, DC 20360
1	Commander Naval Sea Systems Command ATTN: Code SEA-62R Department of the Navy Washington, DC 20362-5101
1	Officer-in-Charge Naval Construction Battalion Center Civil Engineering Laboratory ATTN: Code L06C/L08A (Tech Lib) Port Hueneme, CA 93041
1	Commander David W. Taylor Naval Ship Research & Development Command ATTN: Code 522 (Lib Div) Bethesda, MD 20084-5000
1	Commander Naval Surface Warfare Center ATTN: Code DX-21 (Library) Dahlgren, VA 22448-5000
1	Officer in Charge White Oak Warfare Center Detachment Code E232 (Tech Library) 10901 New Hampshire Ave Silver Spring, MD 20903-5000
1	Commanding Officer White Oak Warfare Center ATTN: Code WA501 (NNPO) Silver Spring, MD 20902-5000
1	Commander (Code 533) Naval Weapons Center China Lake, CA 93555-6001
1	Commander Naval Weapons Evaluation Fac ATTN: Document Control Kirtland AFB, NM 87117
1	Commander Naval Research Laboratory ATTN: Code 2027, Tech Library Washington, DC 20375
2	Air Force Armament Laboratory ATTN: AFATL/DOIL AFATL/DLYV Eglin AFB, FL 32542-5000
1	AFESC/RDCS ATTN: Paul Rosengren Tyndall AFB, FL 32403
1	RADC (EMTLD/Docu Library) Griffiss AFB, NY 13441

DISTRIBUTION LIST

No. of Copies	Organization
3	Air Force Weapons Laboratory ATTN: NTE NTED NTES Kirtland AFB, NM 87117-6008
1	Commander-in-Chief Strategic Air Command ATTN: NRI-STINFO Lib Offutt AFB, NB 68113
1	AFIT ATTN: Tech Lib (Bldg. 640/B) Wright-Patterson AFB, OH 45433
1	AL/LSCF ATTN: J. Levine Edwards AFB, CA 93523-5000
1	AL/TSTL (Tech. Lib.) ATTN: J. Lamb Edwards AFB, CA 93523-5000
1	FTD/NIIS Wright-Patterson AFB Ohio 45433
1	U.S. Department of Energy Idaho Operations Office ATTN: Spec Programs (J. Patton) 785 DOE Place Idaho Falls, ID 83402
2	Director Idaho National Engineering Laboratory EG&G Idaho Inc. ATTN: Mr. R. Guenzler, MS-3505 Mr. R. Holman, MS-3510 P.O. Box 1625 Idaho Falls, ID 83415
1	Director Lawrence Livermore Lab. ATTN: Tech Info Dept L-3 P.O. Box 808 Livermore, CA 94550
2	Director Los Alamos Scientific Lab. ATTN: Mr. Th. Dowler, MS-F602 Doc Control for Reports Library P.O. Box 1663 Los Alamos, NM 87545
3	Director Sandia Laboratories ATTN: Doc Control 3141 Mr. C. Cameron, Div 6215 Mr. A. Chabai, Div 7112 P.O. Box 5800 Albuquerque, NM 87185-5800
1	Director Sandia Laboratories Livermore Laboratory ATTN: Doc Control for Tech Library P.O. Box 969 Livermore, CA 94550
1	Director National Aeronautics and Space Administration ATTN: Scientific & Tech Info Fac P.O. Box 8757, BWI Airport Baltimore, MD 21240
1	Director NASA-Langley Research Center ATTN: Tech Lib Hampton, VA 23665
1	Director NASA-Ames Research Center Applied Computational Aerodynamics Branch ATTN: MS 202-14, Dr. T. Holtz Moffett Field, CA 94035
2	Applied Research Associates, Inc. ATTN: J. Keefer N.H. Ethridge P.O. Box 548 Aberdeen, MD 21001

DISTRIBUTION LIST

No. of Copies	Organization
1	Aerospace Corporation ATTN: Tech Info Services P.O. Box 92957 Los Angeles, CA 90009
1	Agbabian Associates ATTN: M. Agbabian 250 North Nash Street El Segundo, CA 90245
1	Applied Research Associates, Inc. ATTN: R. L. Guice 7114 West Jefferson Ave., Suite 305 Lakewood, CO 80235
1	Black & Veach, Engineers - Arcitects ATTN: Mr. H. D. Laverentz 1500 Meadow Lake Parkway Kansas City, MO 64114
1	The Boeing Company ATTN: Aerospace Library P.O. Box 3707 Seattle, WA 98124
1	California Research & Technology, Inc. ATTN: M. Rosenblatt 20943 Devonshire Street Chatsworth, CA 91311
1	Carpenter Research Corporation ATTN: H. Jerry Carpenter 27520 Hawthorne Blvd., Suite 263 P. O. Box 2490 Rolling Hills Estates, CA 90274
1	Dynamics Technology, Inc. ATTN: D. T. Hove Suite 300 21311 Hawthorne Blvd. Torrance, CA 90503
1	EATON Corporation Defense Valve & Actuator Div. ATTN: Mr. J. Wada 2338 Alaska Ave. El Segundo, CA 90245-4896
1	Goodyear Aerospace Corporation ATTN: R. M. Brown, Bldg 1 Shelter Engineering Litchfield Park, AZ 85340
4	Kaman AviDyne ATTN: Dr. R. Ruetenik (2 cys) Mr. S. Criscione Mr. R. Milligan 83 Second Avenue Northwest Industrial Park Burlington, MA 01830
3	Kaman Sciences Corporation ATTN: Library P. A. Ellis F. H. Shelton 1500 Garden of the Gods Road Colorado Springs, CO 80907
1	Kaman Sciences Corporation ATTN: Mr. F. W. Balicki 6400 Uptown Boulevard N.E. Suite 300 Albuquerque, NM 87110
2	Kaman-TEMPO ATTN: DASIAC Don Sachs P.O. Drawer QQ 816 State Street Santa Barbara, CA 93102
1	Lockheed Missiles & Space Co. ATTN: J. J. Murphy, Dept. 81-11, Bldg. 154 P.O. Box 504 Sunnyvale, CA 94086

DISTRIBUTION LIST

No. of Copies	Organization
2	McDonnell Douglas Astronautics Corporation ATTN: Robert W. Halprin K.A. Heinly 5301 Bolsa Avenue Huntington Beach, CA 92647
2	Physics International Corporation 2700 Merced Street San Leandro, CA 94577
2	R&D Associates ATTN: Technical Library Dr. Allan Kuhl P.O. Box 9695 Marina Del Rey, CA 90291
1	R&D Associates ATTN: G.P. Ganong P.O. Box 9330 Albuquerque, NM 87119
3	Science Applications International Corporation ATTN: Division 164, MST-3-2 W. Layson John Cockayne P.O. BOX 1303 1710 Goodridge Drive McLean, VA 22102
1	Science Applications International Corporation ATTN: Mr. J. Guest 2109 Air Park Road SE Albuquerque, NM 87106
1	Science Applications International Corporation ATTN: Mr. N. Sinha Research Park 202 Wall Street Princeton, NJ 08540-1512
1	Sparta, Inc. Los Angeles Operations ATTN: I. B. Osofsky 3440 Carson Street Torrance, CA 90503
1	Sverdrup Technology, Inc. ATTN: R. F. Starr P. O. Box 884 Tullahoma, TN 37388
1	SRI International ATTN: Dr. G. R. Abrahamson 333 Ravenswood Avenue Menlo Park, CA 94025
2	S-CUBED ATTN: C. E. Needham Lynn Kennedy 2501 Yale Blvd. SE Albuquerque, NM 87106
3	S-CUBED ATTN: Technical Library R. Duff K. Pyatt PO Box 1620 La Jolla, CA 92037-1620
1	Texas Engineering Experiment Station ATTN: Dr. D. Anderson 301 Engineering Research Center College Station, TX 77843
1	Thermal Science, Inc. ATTN: R. Feldman 2200 Cassens Dr. St. Louis, MO 63026
1	TRW - Ballistic Missile Division ATTN: H. Korman, Mail Station 526/614 P.O. Box 1310 San Bernadino, CA 92402
1	Battelle Memorial Institute ATTN: Technical Library 505 King Avenue Columbus, OH 43201

DISTRIBUTION LIST

No. of Copies — Organization

1 California Institute of Technology
ATTN: T. J. Ahrens
1201 E. California Blvd.
Pasadena, CA 91109

2 Denver Research Institute
ATTN: Mr. J. Wisotski
Technical Library
P.O. Box 10758
Denver, CO 80210

1 Massachusetts Institute of Technology
Aeroelastic and Structures Research Laboratory
ATTN: Dr. E. A. Witmer
Cambridge, MA 02139

1 Massachusetts Institute of Technology
ATTN: Technical Library
Cambridge, MA 02139

2 New Mexico Engineering Research Institute (CERF)
University of New Mexico
ATTN: Dr. J. Leigh
Dr. R. Newell
P.O. Box 25
Albuquerque, NM 87131

1 Northrop University
ATTN: Dr. F. B. Safford
5800 W. Arbor Vitae St.
Los Angeles, CA 90045

2 Southwest Research Institute
ATTN: Dr. W. E. Baker
A. B. Wenzel
8500 Culebra Road
San Antonio, TX 78228

1 Stanford University
ATTN: Dr. D. Bershader
Durand Laboratory
Stanford, CA 94305

Aberdeen Proving Ground

Cdr, USATECOM
ATTN: AMSTE-TE-F (L. Teletski)

Cdr, USATHMA
ATTN: AMXTH-TE

Cdr, CSTA
ATTN: STECS-LI

USER EVALUATION SHEET/CHANGE OF ADDRESS

This Laboratory undertakes a continuing effort to improve the quality of the reports it publishes. Your comments/answers to the items/questions below will aid us in our efforts.

1. BRL Report Number BRL-TR-3147 Date of Report SEPTEMBER 1990

2. Date Report Received _____

3. Does this report satisfy a need? (Comment on purpose, related project, or other area of interest for which the report will be used.) _____

4. Specifically, how is the report being used? (Information source, design data, procedure, source of ideas, etc.) _____

5. Has the information in this report led to any quantitative savings as far as man-hours or dollars saved, operating costs avoided, or efficiencies achieved, etc? If so, please elaborate. _____

6. General Comments. What do you think should be changed to improve future reports? (Indicate changes to organization, technical content, format, etc.) _____

CURRENT ADDRESS

_____
Name

_____
Organization

_____
Address

_____
City, State, Zip Code

7. If indicating a Change of Address or Address Correction, please provide the New or Correct Address in Block 6 above and the Old or Incorrect address below.

OLD ADDRESS

_____
Name

_____
Organization

_____
Address

_____
City, State, Zip Code

(Remove this sheet, fold as indicated, staple or tape closed, and mail.)

FOLD HERE

DEPARTMENT OF THE ARMY

Director
U.S. Army Ballistic Research Laboratory
ATTN: SLCBR-DD-T
Aberdeen Proving Ground, MD 21[illegible]5066
OFFICIAL BUSINESS

NO POSTAGE
NECESSARY
IF MAILED
IN THE
UNITED STATES

BUSINESS REPLY MAIL
FIRST CLASS PERMIT No 0001 APG, MD

POSTAGE WILL BE PAID BY ADDRESSEE

Director
U.S. Army Ballistic Research Laboratory
ATTN: SLCBR-DD-T
Aberdeen Proving Ground, MD 21005-9989

FOLD HERE